DYNAMICS & CONTROL OF UNDERWATER GLIDERS II: MOTION PLANNING AND CONTROL

N. Mahmoudian & C. Woolsey

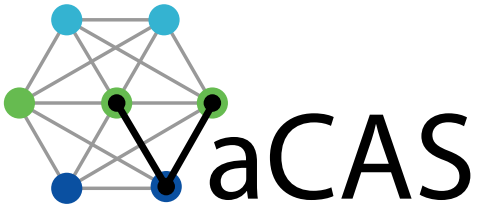

Virginia Center for Autonomous Systems
Virginia Polytechnic Institute & State University
Blacksburg, VA 24060
www.unmanned.vt.edu

November 11, 2010

Technical Report No. VaCAS-2010-2

Summary

This paper describes an underwater glider motion control system intended to enhance locomotive efficiency by reducing the energy expended by vehicle guidance and control. In previous work, the authors derived an approximate analytical expression for steady turning motion by applying regular perturbation theory to a sophisticated vehicle dynamic model. Using these steady turn solutions, including the special case of wings level glides, one may construct feasible paths for the gliders to follow. Because the turning motion results are only approximate, however, and to compensate for model and environmental uncertainty, one must incorporate feedback to ensure precise path following. This report describes the development and numerical implementation of a feedforward/feedback motion control system for a multi-body underwater glider model. Since the motion control system relies largely on steady motions, it is intrinsically efficient. Moreover, the nature of the steady turn approximations suggests a method for nearly energy-optimal path planning.

Contents

List of Figures

1 Introduction

An underwater glider is a winged autonomous underwater vehicle which modulates its buoyancy to rise or sink. It uses servo-actuators to shift the center of mass relative to the center of buoyancy to control pitch and roll attitude. By appropriately cycling these actuators, an underwater glider can control its directional motion and propel itself with great efficiency. Applications include long-term, basin-scale oceanographic sampling and littoral surveillance. The first generation of underwater gliders includes *Slocum* [26], *Seaglider* [4], and *Spray* [25]. (Figure 1 shows a solid model of the *Slocum* gilder.) These "legacy gliders" have proven their worth as efficient, long-distance, long-endurance ocean sampling platforms. They can be deployed for months and travel thousands of kilometers. For example, researchers with the Rutgers University Coastal Ocean Observation Lab (RU-COOL) flew battery powered *Slocum* Gliders over 62000 km, in partnership with Teledyne Webb Research, in different endurance flights [14]. The RU27 *Scarlet Knight* completed a 7410 km mission across the Atlantic on December 4, 2009, completing the unfinished voyage of RU17 which set a record breaking distance of 5700 km during a five-month flight [22]. A University of Washington *Seaglider* remained at sea for six months as it made round trips hundreds of miles in length under the Arctic ice [12]. The exceptional endurance of underwater gliders is due to

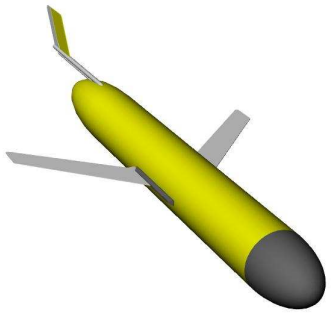

Figure 1: The underwater glider *Slocum* solid model in Rhinoceros 3.0 [7]
Mass 50 (kg); Length 1.5 (m); Wing Span 1 (m); Diameter 0.2 (m).

their reliance on gravity (weight and buoyancy) for propulsion and attitude control. Early efforts in control of buoyancy driven vehicles focused on designing efficient steady motions and controlling the vehicles about these nominal motions [6], but later efforts focused on improving the energy efficiency and controller accuracy of the motion control system [1] and [13]. Results of studies demonstrated the potential for improvements in the current controller design even within the current control structure ([1] and [13]). Classical proportional-integral-derivative (PID) controllers are commonly used for attitude control. These controllers are tuned based on experience and field-tests by the designers and operators of the gliders. (See [1], [2], and [13], for example.) A systematic approach to design a controller using standard linear optimal control design method (linear quadratic regulator (LQR)) was presented in [8] and [17]. Different actuator configurations (pure torque, buoyancy, and elevator control) were considered in [2] and a Lyapunov-based stability result was used to develop control laws for stabilizing desired steady glides.

Leonard and Graver in [8] and [17] mentioned the potential value of "complementing the feedback law with a feedforward term which drives the movable mass and the variable mass in a predetermined way from initial to final condition" in control of underwater gliders. We consider a feedforward/feedback structure for the motion control system as explained in [20]. The feedforward term drives the servo-actuators to predetermined equilibrium positions and the buoyancy bladder to a

predetermined equilibrium obtained from the analytical solution presented in [19], corresponding to some desired steady flight condition. The feedback term compensates for the errors due to the approximation and environmental uncertainty. Steady motions can then be concatenated to achieve compatible guidance objectives, such as waypoint following.

Our aim is to develop implementable, energy-efficient motion control strategies that further improve the inherent efficiency of underwater gliders. Section 2 describes a general dynamic model for an underwater glider. Section 3 reviews the conditions for wings-level gliding flight given in [9] and the approximate conditions for steady turning flight developed in [19]. The motion control system design is presented in Section 4 and the stability of the closed loop system is analyzed in Section 8. Simulation results for the *Slocum* model given in [2] are presented in Section 9. Conclusions of the work and a description of ongoing research are provided in Section 10. More detail can be found in [21].

2 Vehicle Dynamic Model with Actuator Dynamics

The glider is modeled as a rigid body (mass m_{rb}) with two moving mass actuators (m_{px} and m_{py}) and a variable ballast actuator (m_{b}). The total vehicle mass is

$$m_{\mathrm{v}} = m_{\mathrm{rb}} + m_{\mathrm{px}} + m_{\mathrm{py}} + m_{\mathrm{b}},$$

where m_{b} can be modulated by control.

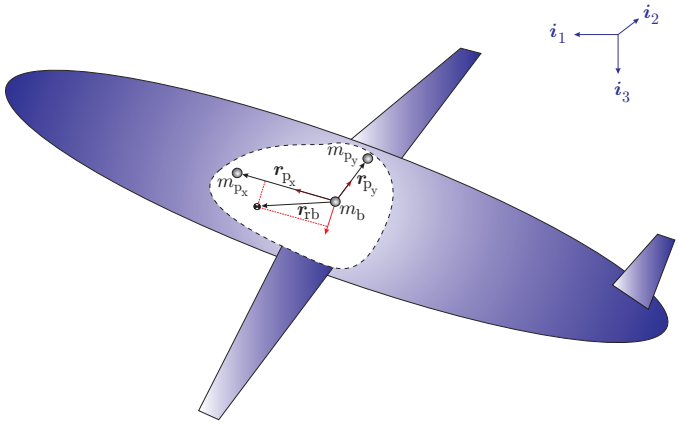

Figure 2: Illustration of point mass actuators.

The vehicle displaces a volume of fluid of mass m. If $\tilde{m} := m_{\mathrm{v}} - m$ is greater than zero, the vehicle is heavy in water and tends to sink while if $\tilde{m}$ is negative, the vehicle is buoyant in water and tends to rise. Figure 2 shows the simplified model for the underwater glider actuation system. The variable mass is represented by a mass particle m_{b} located at the origin of a body-fixed reference frame.

The vehicle's attitude is given by a proper rotation matrix $\boldsymbol{\mathcal{R}}_{\mathrm{IB}}$ which maps free vectors from the body-fixed reference frame to a reference frame fixed in inertial space. The body frame is defined by an orthonormal triad $\{\boldsymbol{b}_1, \boldsymbol{b}_2, \boldsymbol{b}_3\}$, where $\boldsymbol{b}_1$ is aligned with the body's longitudinal axis. The origin of a body-fixed reference frame is located at the center of volume of the vehicle as illustrated in Figure 2. The inertial frame is represented by an orthonormal triad $\{\boldsymbol{i}_1, \boldsymbol{i}_2, \boldsymbol{i}_3\}$, where $\boldsymbol{i}_3$ is aligned

with the local direction of gravity. To define the rotation matrix explicitly, let vectors $\boldsymbol{e}_i$ define the standard basis for $\mathbb{R}^3$ for $i \in \{1, 2, 3\}$:

$$\boldsymbol{e}_1 = \begin{pmatrix} 1 \\ 0 \\ 0 \end{pmatrix}, \quad \boldsymbol{e}_2 = \begin{pmatrix} 0 \\ 1 \\ 0 \end{pmatrix}, \quad \text{and} \quad \boldsymbol{e}_3 = \begin{pmatrix} 0 \\ 0 \\ 1 \end{pmatrix}$$

Also, let the character $\hat{\cdot}$ denote the 3×3 skew-symmetric matrix satisfying $\hat{\boldsymbol{a}}\boldsymbol{b} = \boldsymbol{a} \times \boldsymbol{b}$ for 3-vectors $\boldsymbol{a}$ and $\boldsymbol{b}$. The rotation matrix $\boldsymbol{\mathcal{R}}_{\text{IB}}$ is typically parameterized using the roll angle ϕ, pitch angle θ, and yaw angle ψ:

$$\boldsymbol{\mathcal{R}}_{\text{IB}}(\phi, \theta, \psi) = e^{\widehat{\boldsymbol{e}_3}\psi} e^{\widehat{\boldsymbol{e}_2}\theta} e^{\widehat{\boldsymbol{e}_1}\phi} \qquad \text{where} \qquad e^{\boldsymbol{Q}} = \sum_{n=0}^{\infty} \frac{1}{n!} \boldsymbol{Q}^n \quad \text{for} \quad \boldsymbol{Q} \in \mathbb{R}^{n \times n}.$$

Let $\boldsymbol{v} = [u,\ v,\ w]^T$ represent the translational velocity and let $\boldsymbol{\omega} = [p,\ q,\ r]^T$ represent the rotational velocity of the underwater glider with respect to inertial space, where $\boldsymbol{v}$ and $\boldsymbol{\omega}$ are both expressed in the body frame. Letting $\boldsymbol{y}$ represent the position of the body frame origin with respect to the inertial frame, the vehicle kinematic equations are

$$\dot{\boldsymbol{y}} = \boldsymbol{\mathcal{R}}_{\text{IB}} \boldsymbol{v} \tag{1}$$

$$\dot{\boldsymbol{\mathcal{R}}}_{\text{IB}} = \boldsymbol{R}_{\text{IB}} \hat{\boldsymbol{\omega}}. \tag{2}$$

In terms of these Euler angles, the kinematic equations (1) and (2) become, respectively,

$$\begin{pmatrix} \dot{x} \\ \dot{y} \\ \dot{z} \end{pmatrix} = \begin{pmatrix} \cos\theta\cos\psi & \sin\phi\sin\theta\cos\psi - \cos\phi\sin\psi & \cos\phi\sin\theta\cos\psi + \sin\phi\sin\psi \\ \cos\theta\sin\psi & \cos\phi\cos\psi + \sin\phi\sin\theta\sin\psi & -\sin\phi\cos\psi + \cos\phi\sin\theta\sin\psi \\ -\sin\theta & \sin\phi\cos\theta & \cos\phi\cos\theta \end{pmatrix} \begin{pmatrix} u \\ v \\ w \end{pmatrix}$$

$$\begin{pmatrix} \dot{\phi} \\ \dot{\theta} \\ \dot{\psi} \end{pmatrix} = \begin{pmatrix} 1 & \sin\phi\tan\theta & \cos\phi\tan\theta \\ 0 & \cos\phi & -\sin\phi \\ 0 & \sin\phi\sec\theta & \cos\phi\sec\theta \end{pmatrix} \begin{pmatrix} p \\ q \\ r \end{pmatrix}.$$

As indicated in Figure 2, the mass particle m_{p_x} is constrained to move along the longitudinal axis while the mass particle m_{p_y} is constrained to move along the lateral axis:

$$\boldsymbol{r}_{\text{p}_\text{x}} = r_{\text{p}_\text{x}} \boldsymbol{e}_1 \quad \text{and} \quad \boldsymbol{r}_{\text{p}_\text{y}} = r_{\text{p}_\text{y}} \boldsymbol{e}_2$$

Following [27], define the mass, inertia, and inertial coupling matrices for the combined rigid body/moving mass/variable ballast system as

$$\begin{aligned} \boldsymbol{I}_{\text{rb/p/b}} &= \boldsymbol{I}_{\text{rb}} - m_{\text{p}_\text{x}} \hat{\boldsymbol{r}}_{\text{p}_\text{x}} \hat{\boldsymbol{r}}_{\text{p}_\text{x}} - m_{\text{p}_\text{y}} \hat{\boldsymbol{r}}_{\text{p}_\text{y}} \hat{\boldsymbol{r}}_{\text{p}_\text{y}} \\ \boldsymbol{M}_{\text{rb/p/b}} &= m_{\text{v}} \mathbb{I} \\ \boldsymbol{C}_{\text{rb/p/b}} &= m_{\text{rb}} \hat{\boldsymbol{r}}_{\text{rb}} + m_{\text{p}_\text{x}} \hat{\boldsymbol{r}}_{\text{p}_\text{x}} + m_{\text{p}_\text{y}} \hat{\boldsymbol{r}}_{\text{p}_\text{y}} \end{aligned}$$

where $\mathbb{I}$ represents the 3×3 identity matrix. The rigid body inertia matrix $\boldsymbol{I}_{\text{rb}}$ represents the distribution of mass m_{rb} and is assumed to take the form

$$\boldsymbol{I}_{\text{rb}} = \begin{pmatrix} I_{xx} & 0 & -I_{xz} \\ 0 & I_{yy} & 0 \\ -I_{xz} & 0 & I_{zz} \end{pmatrix}$$

where the off-diagonal terms in $\boldsymbol{I}_{\text{rb}}$ arise, for example, from an offset center of mass $\boldsymbol{r}_{\text{rb}} = [x_{\text{rb}}, 0, z_{\text{rb}}]^T$. It is notationally convenient to compile the various inertia matrices into the *generalized* inertia matrix $\mathbb{M}_{\text{rb/p/b}}$.

$$\mathbb{M}_{\text{rb/p/b}} = \begin{pmatrix} \boldsymbol{I}_{\text{rb/p/b}} & \boldsymbol{C}_{\text{rb/p/b}} & m_{\text{p}_\text{x}} \hat{\boldsymbol{r}}_{\text{p}_\text{x}} \boldsymbol{e}_1 & m_{\text{p}_\text{y}} \hat{\boldsymbol{r}}_{\text{p}_\text{y}} \boldsymbol{e}_2 \\ \boldsymbol{C}^T_{\text{rb/p/b}} & \boldsymbol{M}_{\text{rb/p/b}} & m_{\text{p}_\text{x}} \boldsymbol{e}_1 & m_{\text{p}_\text{y}} \boldsymbol{e}_2 \\ -m_{\text{p}_\text{x}} \boldsymbol{e}_1^T \hat{\boldsymbol{r}}_{\text{p}_\text{x}} & m_{\text{p}_\text{x}} \boldsymbol{e}_1^T & m_{\text{p}_\text{x}} & 0 \\ -m_{\text{p}_\text{y}} \boldsymbol{e}_2^T \hat{\boldsymbol{r}}_{\text{p}_\text{y}} & m_{\text{p}_\text{y}} \boldsymbol{e}_2^T & 0 & m_{\text{p}_\text{y}} \end{pmatrix}$$

The generalized *added* inertia matrix is composed of the added mass matrix $\boldsymbol{M}_{\text{f}}$, the added inertia matrix $\boldsymbol{I}_{\text{f}}$, and the added inertial coupling matrix $\boldsymbol{C}_{\text{f}}$:

$$\mathbb{M}_{\text{f}} = \begin{pmatrix} \boldsymbol{I}_{\text{f}} & \boldsymbol{C}_{\text{f}} & \mathbb{O}_{3\times 2} \\ \boldsymbol{C}^T_{\text{f}} & \boldsymbol{M}_{\text{f}} & \mathbb{O}_{3\times 2} \\ \mathbb{O}_{2\times 3} & \mathbb{O}_{2\times 3} & \mathbb{O}_{2\times 2} \end{pmatrix}$$

The generalized added inertia matrix accounts for the energy necessary to accelerate the fluid around the vehicle as it rotates and translates. In notation similar to that defined by SNAME [5][1],

$$\left(\begin{array}{c|c} \boldsymbol{I}_{\text{f}} & \boldsymbol{C}_{\text{f}} \\ \hline \boldsymbol{C}^T_{\text{f}} & \boldsymbol{M}_{\text{f}} \end{array}\right) = -\left(\begin{array}{ccc:ccc} L_{\dot{p}} & L_{\dot{q}} & L_{\dot{r}} & L_{\dot{u}} & L_{\dot{v}} & L_{\dot{w}} \\ M_{\dot{p}} & M_{\dot{q}} & M_{\dot{r}} & M_{\dot{u}} & M_{\dot{v}} & M_{\dot{w}} \\ N_{\dot{p}} & N_{\dot{q}} & N_{\dot{r}} & N_{\dot{u}} & N_{\dot{v}} & N_{\dot{w}} \\ \hdashline X_{\dot{p}} & X_{\dot{q}} & X_{\dot{r}} & X_{\dot{u}} & X_{\dot{v}} & X_{\dot{w}} \\ Y_{\dot{p}} & Y_{\dot{q}} & Y_{\dot{r}} & Y_{\dot{u}} & Y_{\dot{v}} & Y_{\dot{w}} \\ Z_{\dot{p}} & Z_{\dot{q}} & Z_{\dot{r}} & Z_{\dot{u}} & Z_{\dot{v}} & Z_{\dot{w}} \end{array}\right)$$

The generalized inertia for the vehicle/fluid system is

$$\mathbb{M} = \mathbb{M}_{\text{rb/p/b}} + \mathbb{M}_{\text{f}} = \begin{pmatrix} \boldsymbol{I} & \boldsymbol{C} & m_{\text{p}_\text{x}} \hat{\boldsymbol{r}}_{\text{p}_\text{x}} \boldsymbol{e}_1 & m_{\text{p}_\text{y}} \hat{\boldsymbol{r}}_{\text{p}_\text{y}} \boldsymbol{e}_2 \\ \boldsymbol{C}^T & \boldsymbol{M} & m_{\text{p}_\text{x}} \boldsymbol{e}_1 & m_{\text{p}_\text{y}} \boldsymbol{e}_2 \\ -m_{\text{p}_\text{x}} \boldsymbol{e}_1^T \hat{\boldsymbol{r}}_{\text{p}_\text{x}} & m_{\text{p}_\text{x}} \boldsymbol{e}_1^T & m_{\text{p}_\text{x}} & 0 \\ -m_{\text{p}_\text{y}} \boldsymbol{e}_2^T \hat{\boldsymbol{r}}_{\text{p}_\text{y}} & m_{\text{p}_\text{y}} \boldsymbol{e}_2^T & 0 & m_{\text{p}_\text{y}} \end{pmatrix} \tag{3}$$

where the inertia $\boldsymbol{I}$, mass $\boldsymbol{M}$, and coupling $\boldsymbol{C}$ matrices are defined as follows:

$$\begin{aligned} \boldsymbol{I} &= \boldsymbol{I}_{\text{rb/p/b}} + \boldsymbol{I}_{\text{f}} \\ \boldsymbol{M} &= \boldsymbol{M}_{\text{rb/p/b}} + \boldsymbol{M}_{\text{f}} \\ \boldsymbol{C} &= \boldsymbol{C}_{\text{rb/p/b}} + \boldsymbol{C}_{\text{f}} \end{aligned}$$

Let $\boldsymbol{p}_{\text{sys}}$ represent the total linear momentum of the vehicle/fluid system and $\boldsymbol{h}_{\text{sys}}$ represent the total angular momentum both expressed in the body frame. Let $\boldsymbol{p}_{\text{p}_\text{x}}$ and $\boldsymbol{p}_{\text{p}_\text{y}}$ represent the total translational momentum of the moving mass particles expressed in the body frame. Defining the generalized velocity $\boldsymbol{\eta} = (\ \boldsymbol{\omega}^T \quad \boldsymbol{v}^T \quad \dot{r}_{\text{p}_\text{x}} \quad \dot{r}_{\text{p}_\text{y}}\ )^T$ and the generalized momentum $\boldsymbol{\nu} = (\ \boldsymbol{h}^T_{\text{sys}} \quad \boldsymbol{p}^T_{\text{sys}} \quad p_{\text{p}_\text{x}} \quad p_{\text{p}_\text{y}}\ )^T$, we have

$$\boldsymbol{\nu} = \mathbb{M}\boldsymbol{\eta} \tag{4}$$

[1] In SNAME notation, roll moment is denoted by K rather than L

The dynamic equations in mixed momentum/velocity notation are

$$\begin{aligned}
\dot{\boldsymbol{h}}_{\text{sys}} &= \boldsymbol{h}_{\text{sys}} \times \boldsymbol{\omega} + \boldsymbol{p}_{\text{sys}} \times \boldsymbol{v} + (m_{\text{rb}} g \boldsymbol{r}_{\text{rb}} + m_{\text{p}_\text{x}} g \boldsymbol{r}_{\text{p}_\text{x}} + m_{\text{p}_\text{y}} g \boldsymbol{r}_{\text{p}_\text{y}}) \times (\boldsymbol{\mathcal{R}}_{\text{IB}}^T \boldsymbol{i}_3) + \boldsymbol{T}_{\text{visc}} \\
\dot{\boldsymbol{p}}_{\text{sys}} &= \boldsymbol{p}_{\text{sys}} \times \boldsymbol{\omega} + \tilde{m} g (\boldsymbol{\mathcal{R}}_{\text{IB}}^T \boldsymbol{i}_3) + \boldsymbol{F}_{\text{visc}} \\
\dot{p}_{\text{p}_\text{x}} &= \boldsymbol{e}_1 \cdot \left(\boldsymbol{p}_{\text{p}_\text{x}} \times \boldsymbol{\omega} + m_{\text{p}_\text{x}} g (\boldsymbol{\mathcal{R}}_{\text{IB}}^T \boldsymbol{i}_3) \right) + \tilde{u}_{\text{p}_\text{x}} \\
\dot{p}_{\text{p}_\text{y}} &= \boldsymbol{e}_2 \cdot \left(\boldsymbol{p}_{\text{p}_\text{y}} \times \boldsymbol{\omega} + m_{\text{p}_\text{y}} g (\boldsymbol{\mathcal{R}}_{\text{IB}}^T \boldsymbol{i}_3) \right) + \tilde{u}_{\text{p}_\text{y}} \\
\dot{m}_{\text{b}} &= u_{\text{b}}
\end{aligned} \tag{5}$$

where the terms $\boldsymbol{T}_{\text{visc}}$ and $\boldsymbol{F}_{\text{visc}}$ represent external moments and forces which do not derive from scalar potential functions. These moments and forces include control moments, such as the yaw moment due to a rudder (if present), and viscous forces, such as lift and drag.

The forces $\tilde{u}_{\text{p}_\text{x}}$ and $\tilde{u}_{\text{p}_\text{y}}$ can be chosen to cancel to remaining terms in the equations for $\dot{p}_{\text{p}_\text{x}}$ and $\dot{p}_{\text{p}_\text{y}}$, so that

$$\begin{aligned}
\dot{p}_{\text{p}_\text{x}} &= u_{\text{p}_\text{x}} \\
\dot{p}_{\text{p}_\text{y}} &= u_{\text{p}_\text{y}}.
\end{aligned}$$

The new inputs u_{p_x} and u_{p_y} may then be chosen to servo-actuate the point mass positions for attitude control, subject to limits on point mass position and velocity. (Physically, these actuators might each consist of a large mass m_{p_x} or m_{p_y} mounted on a power screw that is driven by a servomotor.) The mass flow rate u_{b} is chosen to servo-actuate the vehicle's net weight, again subject to control magnitude and rate limits. These magnitude and rate limits are significant for underwater gliders and must be considered in control design and analysis.

The viscous forces and moments are expressed in terms of the hydrodynamic angles

$$\alpha = \arctan\left(\frac{w}{u}\right) \qquad \text{and} \qquad \beta = \arcsin\left(\frac{v}{V}\right)$$

where $V = \|\boldsymbol{v}\|$. The viscous force and moment are most easily expressed in the "current" reference frame. This frame is related to the body frame through the proper rotation

$$\boldsymbol{\mathcal{R}}_{\text{BC}}(\alpha, \beta) = e^{-\widehat{\boldsymbol{e}_2}\alpha} e^{\widehat{\boldsymbol{e}_3}\beta} = \begin{pmatrix} \cos\alpha\cos\beta & -\cos\alpha\sin\beta & -\sin\alpha \\ \sin\beta & \cos\beta & 0 \\ \sin\alpha\cos\beta & -\sin\alpha\sin\beta & \cos\alpha \end{pmatrix}.$$

For example, one may write

$$\boldsymbol{v} = \boldsymbol{\mathcal{R}}_{\text{BC}}(\alpha, \beta)(V \boldsymbol{e}_1) = \begin{pmatrix} V\cos\alpha\cos\beta \\ V\sin\beta \\ V\sin\alpha\cos\beta \end{pmatrix}.$$

Following standard modeling conventions, we write

$$\boldsymbol{F}_{\text{visc}} = -\boldsymbol{\mathcal{R}}_{\text{BC}}(\alpha, \beta) \begin{pmatrix} \mathcal{D}(\alpha) \\ \mathcal{S}_\beta \beta + S_{\delta r} \delta r \\ \mathcal{L}_\alpha \alpha \end{pmatrix} \qquad \text{and} \qquad \boldsymbol{T}_{\text{visc}} = \boldsymbol{D}_\omega \boldsymbol{\omega} + \begin{pmatrix} L_\beta \beta \\ M_\alpha \alpha \\ N_\beta \beta + N_{\delta r} \delta r \end{pmatrix}$$

where $\mathcal{D}$, $\mathcal{S}$, and $\mathcal{L}$ represent drag, side force, and lift, respectively, L, M, and N represent roll, pitch, and yaw moment and subscripts denote sensitivities to the indicated variable. The moment $\boldsymbol{D}_\omega \boldsymbol{\omega}$ represents hydrodynamic damping due to vehicle rotation.

Equations (1), (2), and (5) completely describe the motion of an underwater glider in inertial space. In studying steady motions, we typically neglect the translational kinematics (1). Moreover, the structure of the dynamic equations (5) is such that we only need to retain a portion of the rotational kinematics (2). Given the "tilt" vector $\boldsymbol{\zeta} = \boldsymbol{\mathcal{R}}_{\mathrm{IB}}^{T}\boldsymbol{i}_3$ (i.e., the body frame unit vector pointing in the direction of gravity), and referring to equation (2), it is easy to see that $\dot{\boldsymbol{\zeta}} = \boldsymbol{\zeta} \times \boldsymbol{\omega}$. The reduced set of dynamic equations, with buoyancy control and moving mass actuator dynamics explicitly represented, are:

$$\begin{aligned}
\dot{\boldsymbol{h}}_{\mathrm{sys}} &= \boldsymbol{h}_{\mathrm{sys}} \times \boldsymbol{\omega} + \boldsymbol{p}_{\mathrm{sys}} \times \boldsymbol{v} + (m_{\mathrm{rb}} g \boldsymbol{r}_{\mathrm{rb}} + m_{\mathrm{p_x}} g \boldsymbol{r}_{\mathrm{p_x}} + m_{\mathrm{p_y}} g \boldsymbol{r}_{\mathrm{p_y}}) \times \boldsymbol{\zeta} + \boldsymbol{T}_{\mathrm{visc}} \\
\dot{\boldsymbol{p}}_{\mathrm{sys}} &= \boldsymbol{p}_{\mathrm{sys}} \times \boldsymbol{\omega} + \tilde{m} g \boldsymbol{\zeta} + \boldsymbol{F}_{\mathrm{visc}} \\
\dot{\boldsymbol{\zeta}} &= \boldsymbol{\zeta} \times \boldsymbol{\omega} \\
\dot{p}_{\mathrm{p_x}} &= u_{\mathrm{p_x}} \\
\dot{p}_{\mathrm{p_y}} &= u_{\mathrm{p_y}} \\
\dot{m}_{\mathrm{b}} &= u_{\mathrm{b}}
\end{aligned} \tag{6}$$

As mentioned previously, equations (6) are written in mixed velocity/momentum notation. To design a control system, we convert these into a consistent set of state variables by computing

$$\dot{\boldsymbol{\eta}} = \left[\mathbb{M}^{-1}\dot{\boldsymbol{\nu}} - \mathbb{M}^{-1}\dot{\mathbb{M}} \;\; \mathbb{M}^{-1}\boldsymbol{\nu} \right]_{\boldsymbol{\nu}=\mathbb{M}\boldsymbol{\eta}} \tag{7}$$

where $\dot{\mathbb{M}}$ is the time derivative of the generalized inertia:

$$\dot{\mathbb{M}} = \begin{pmatrix}
\dot{\boldsymbol{I}} & \dot{\boldsymbol{C}} & m_{\mathrm{p_x}} \dot{\hat{\boldsymbol{r}}}_{\mathrm{p_x}} \boldsymbol{e}_1 & m_{\mathrm{p_y}} \dot{\hat{\boldsymbol{r}}}_{\mathrm{p_y}} \boldsymbol{e}_2 \\
\dot{\boldsymbol{C}}^{T} & \mathbb{O}_{3\times 3} & 0\boldsymbol{e}_1 & 0\boldsymbol{e}_2 \\
-m_{\mathrm{p_x}} \boldsymbol{e}_1^{T} \dot{\hat{\boldsymbol{r}}}_{\mathrm{p_x}} & 0\boldsymbol{e}_1^{T} & 0 & 0 \\
-m_{\mathrm{p_y}} \boldsymbol{e}_2^{T} \dot{\hat{\boldsymbol{r}}}_{\mathrm{p_y}} & 0\boldsymbol{e}_2^{T} & 0 & 0
\end{pmatrix}$$

with

$$\begin{aligned}
\dot{\boldsymbol{I}} &= -m_{\mathrm{p_x}} (\hat{\boldsymbol{r}}_{\mathrm{p_x}} \dot{\hat{\boldsymbol{r}}}_{\mathrm{p_x}} + \dot{\hat{\boldsymbol{r}}}_{\mathrm{p_x}} \hat{\boldsymbol{r}}_{\mathrm{p_x}}) - m_{\mathrm{p_y}} (\hat{\boldsymbol{r}}_{\mathrm{p_y}} \dot{\hat{\boldsymbol{r}}}_{\mathrm{p_y}} + \dot{\hat{\boldsymbol{r}}}_{\mathrm{p_y}} \hat{\boldsymbol{r}}_{\mathrm{p_y}}) \\
\dot{\boldsymbol{C}} &= m_{\mathrm{p_x}} \dot{\hat{\boldsymbol{r}}}_{\mathrm{p_x}} + m_{\mathrm{p_y}} \dot{\hat{\boldsymbol{r}}}_{\mathrm{p_y}}.
\end{aligned}$$

3 Steady Flight

In wings-level, gliding flight the vehicle has no angular velocity ($\boldsymbol{\omega} = \boldsymbol{0}$), no lateral velocity component ($v = 0$, so that $\beta = 0$), and no roll angle ($\phi = 0$). Also, $r_{\mathrm{p_y}} = 0$ and $\delta r = 0$ (if the vehicle has a rudder). Following the analysis presented in [9], one may compute the required CG location ($\boldsymbol{r}_{\mathrm{rb}}$) and the required net mass $\tilde{m}_0$ for balanced gliding flight at a specified speed and glide path angle. Let γ denote the glide path angle; in wings-level flight, $\gamma = \theta - \alpha$. For steady wings-level flight at a specified speed V_0 and glide path angle $\gamma_0 = \theta_0 - \alpha_0$,

$$\boldsymbol{r}_{\mathrm{rb}} = \frac{1}{m_{\mathrm{rb}} g} \left(\boldsymbol{M}\boldsymbol{v}_0 \times \boldsymbol{v}_0 + \begin{pmatrix} 0 \\ M_\alpha \alpha_0 \\ 0 \end{pmatrix} \right) \times \boldsymbol{\zeta}_0 + \varrho \boldsymbol{\zeta}_0 \tag{8}$$

$$\tilde{m}_0 = \frac{1}{g} \left(\cos(\gamma_0) \mathcal{L}_\alpha \alpha_0 - \sin(\gamma_0) \mathcal{D}(\alpha_0, 0) \right). \tag{9}$$

In the equation for $\boldsymbol{r}_{\text{rb}}$, $\boldsymbol{v}_0 = V_0\,[\cos\alpha_0,\ 0,\ \sin\alpha_0]^T$, $\boldsymbol{\zeta}_0 = [-\sin\theta_0,\ 0,\ \cos\theta_0]^T$, and ϱ is a free parameter related to the vehicle's "bottom-heaviness" in the given flight condition [9]. (Note that, in determining a nominal wings-level glide condition, we assume that $r_{\text{p}_\text{x}} = 0$. That is, the nominal gravitational moment is due entirely to $\boldsymbol{r}_{\text{rb}}$.) Analysis of turning (helical) flight using a sophisticated underwater glider model is challenging. In [19], the problem was formulated as a regular perturbation problem in the turn rate, as represented by a small, non-dimensional turn rate parameter ϵ. In seeking a first order solution for turning flight, it was assumed that the pitch angle remains at its nominal value for wings-level flight (θ_0). Polynomial expansions for r_{p_y}, $\tilde{m}$, ϕ, V, α, and β in terms of ϵ were substituted into the nonlinear algebraic equations for steady turning flight. Solving the coefficient equation for ϵ^1 gives approximate equilibrium values for r_{p_y}, $\tilde{m}$, ϕ, V, α, and β, to first order in ϵ. It was found in [19] that these first order approximate values take the form:

$$\begin{aligned} V_1 &= 0 \\ \alpha_1 &= 0 \\ \tilde{m}_1 &= 0 \\ \beta_1 &= \beta_1(\alpha_0, \theta_0, \tilde{m}_0; \delta_{r_1}) \\ \phi_1 &= \phi_1(\alpha_0, \theta_0, \tilde{m}_0; \beta_1, \delta_{r_1}) \\ r_{\text{p}_{\text{y}_1}} &= r_{\text{p}_{\text{y}_1}}(\alpha_0, \theta_0, \tilde{m}_0; \delta_{r_1}) \end{aligned} \tag{10}$$

Explicit expressions for β_1, ϕ_1, and $r_{\text{p}_{\text{y}_1}}$ are given in [19]. The approximate solution indicated in (10) shows that V, α, and $\tilde{m}$ remain constant to first order in ϵ. This suggests that the primary contributors to steady turning motion are lateral mass deflections (r_{p_y}) and rudder deflections (δr) and that these deflections have no first order effect on speed or angle of attack. In practice, it is considerably more costly to change the vehicle's net mass $\tilde{m}$ than to shift its CG, so it is fortunate that turning motions at the same (approximate) speed and glide path angle can be obtained by only varying r_{p_y} and/or δ_r. These observations suggest a natural approach to motion control for underwater gliders: Fix the buoyancy and center of gravity for a desired, wings level flight condition and then use the lateral moving mass actuator to control turn rate and longitudinal moving mass actuator to control flight path angle.

4 Motion Control System

Having characterized steady, wings level flight and steady turning motions (at least approximately), as described in Section 3, one can formulate a motion control strategy which relies on these solutions. The aim is to track inputs of constant desired speed (V_d), glide path angle (γ_d), and turn rate ($\dot{\psi}_\text{d}$). Given feasible values for desired speed, glide path angle, and turn rate, one may compute feedforward actuator commands to adjust the net weight and center of gravity in order to achieve the given flight condition. Because these values are only approximate, though, and because of modeling and environmental uncertainty, the commanded values must be augmented using feedback compensation. The design and analysis of such a feedforward/feedback motion control system requires a model that incorporates buoyancy and moving mass actuator dynamics as presented in Section 2.

An illustration of such a feedforward/feedback control system is shown in Figure 3. The vector field $\boldsymbol{f}(\boldsymbol{x}, \boldsymbol{u})$ represents the system dynamics with state vector $\boldsymbol{x}$ and inputs $\boldsymbol{u}$, and the vector field $\tilde{\boldsymbol{f}}(\boldsymbol{x}, \boldsymbol{u})$ notionally represents their first order approximation in turn rate. The pair $(\tilde{\boldsymbol{x}}_{\text{eq}}, \tilde{\boldsymbol{u}}_{\text{eq}})$

represents the first order solution for a given desired steady motion. The vector $\boldsymbol{\mu}$ contains parameter values which, if held constant, correspond to some stable steady motion. Such a feedforward/feedback motion control system was briefly presented in [20]; a more thorough discussion of the design and analysis was presented [18].

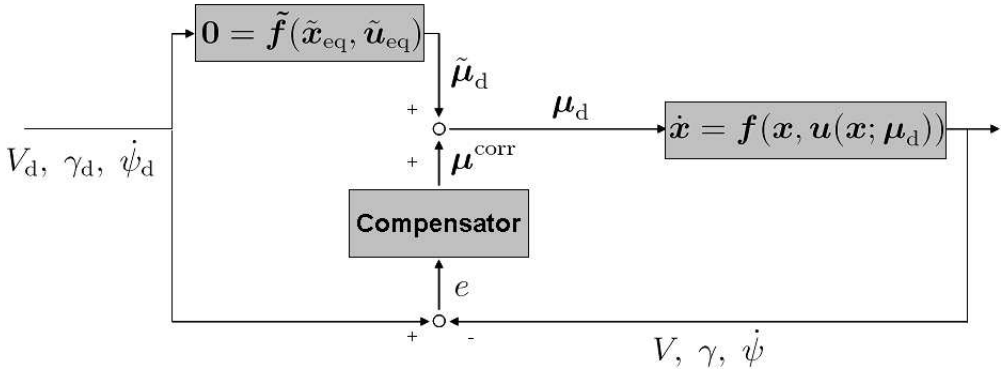

Figure 3: A steady motion-based feedforward/feedback control system.

The first step in the motion control scheme is to obtain the parameter values $\tilde{\boldsymbol{\mu}}_{\mathrm{d}}$ (net mass and moving mass positions) that correspond to the desired steady motion $\tilde{\boldsymbol{x}}_{\mathrm{eq}}$ (characterized by V_{d}, γ_{d}, and $\dot{\psi}_{\mathrm{d}}$), to first order in turn rate. This inverse problem is expressed notionally in the feedforward block in Figure 3 by the equation

$$\mathbf{0} = \tilde{\boldsymbol{f}}(\tilde{\boldsymbol{x}}_{\mathrm{eq}}, \tilde{\boldsymbol{u}}_{\mathrm{eq}}),$$

which was solved analytically for the corresponding parameter values $\tilde{\boldsymbol{\mu}}_{\mathrm{d}}$ in [19].

The feedback block compensates for the error due to the approximation and environmental uncertainty, adding a correction denoted $\boldsymbol{\mu}^{\mathrm{corr}}$.

The feedback-compensated "parameter commands" $\boldsymbol{\mu}_{\mathrm{d}}$ are then realized within the vehicle dynamics

$$\dot{\boldsymbol{x}} = \boldsymbol{f}(\boldsymbol{x}; \boldsymbol{u}(\boldsymbol{x}; \boldsymbol{\mu}_{\mathrm{d}}))$$

through an appropriately designed servo-control system. Here, $\boldsymbol{u}$ is a feedback control law that attempts to maintain commanded parameter values $\boldsymbol{\mu}_{\mathrm{d}}$ in spite of the vehicle dynamics.

The control system depicted in Figure 3 suggests that one may vary the steady motion, according to some desired guidance objective. However, one must verify that the closed loop system is stable. Fixing parameter values, one may examine open-loop stability by linearizing about the approximate equilibrium conditions and computing the eigenvalues of the state matrix. Because eigenvalues depend continuously on the state matrix parameters, stability of the true equilibrium may be inferred from stability of the approximate equilibrium provided (i) the equilibrium is hyperbolic and (ii) ϵ is small relative to the magnitude of the real part of each eigenvalue. (See Section 1.7 of [10] or Chapter 9 of [11] for more details.) Given that the system does possess a stable, steady motion parameterized by a set of commanded parameter values, one must still verify that the system remains stable while varying these parameter values. For example, if one changes the reference commands in Figure 3 too rapidly, one might drive the nonlinear system unstable.

As explained earlier, underwater gliders steer by moving one or more internal masses. The vehicle dynamics are quite slow, relative to the actuator dynamics. Commanding a rapid change in turn rate, for example, will result in a quick change in center of mass location, but the resulting effect

on the vehicle's motion will be much slower. Alternatively, one may issue reference commands that vary "quasisteadily" and treat the closed-loop system as "slowly varying" in the turn rate $\dot{\psi}_{\rm d}(t)$. We may then analyze stability of the closed loop system in the context of slowly varying systems theory [15].

Suppose the output of a nonlinear system

$$\dot{\boldsymbol{x}} = f(\boldsymbol{x}, u_{\rm py}) \; ; \quad u_{\rm py} = \kappa(\boldsymbol{x}, \dot{\psi}_{\rm d})$$

is required to track a reference input $\dot{\psi}_{\rm d}(t)$, where the feedback controller κ is designed such that the closed-loop system has a locally exponentially stable equilibrium at $\boldsymbol{x}_{\rm eq}$ when $\dot{\psi}_{\rm d}(t)$ is constant. The turn rate $\dot{\psi}_{\rm d}(t)$ is called "slowly varying" if it is continuously differentiable and, for some sufficiently small $\varepsilon > 0$, one has $\|\ddot{\psi}_{\rm d}(t)\| \leq \varepsilon$ for all $t \geq 0$.

We will analyze the underwater glider's motion control system using slowly varying systems theory to prove stability of the closed-loop system and, simultaneously, to determine how fast one may vary the commanded turn rate and maintain stability.

Following Khalil [15] (Chapter 9), to analyze this system, consider $\dot{\psi}_{\rm d}$ as a "frozen" parameter and assume that for each fixed value the frozen system has an isolated equilibrium point defined by $\boldsymbol{x}_{\rm eq} = \mathbf{h}(\dot{\psi}_{\rm d})$ where $\|\frac{\partial \mathbf{h}}{\partial \dot{\psi}_{\rm d}}\| \leq L$. To analyze stability of the frozen equilibrium point, we shift it to the origin via the change of the variables $\acute{\boldsymbol{x}} = \boldsymbol{x} - \mathbf{h}(\dot{\psi}_{\rm d})$ to obtain equation

$$\dot{\acute{\boldsymbol{x}}} = g(\acute{\boldsymbol{x}})$$

Based on Theorem 9.3 of Khalil [15], if there is a positive definite and decrescent Lyapunov function $V(\acute{\boldsymbol{x}})$ which satisfies certain properties, the trajectory $\acute{\boldsymbol{x}}(t)$ will be uniformly ultimately bounded. Moreover, if $\ddot{\psi}_{\rm d}(t) \to 0$ as $t \to \infty$, then the tracking error tends to zero. Details of the analysis are provided in Section 8.

5 Feedforward/Feedback Controller Design

The feedforward block takes the commanded steady motion parameters (speed, glide path angle, and turn rate) and generates the corresponding values for buoyancy and center of mass location, as predicted by perturbation analysis. Because the turning motion results are only approximate, however, and to compensate for model and environmental uncertainty, we incorporate feedback. The objective here is to design single-input, single-output PID control loops to *modify* the feedforward commands based on measured errors in the values of speed V, glide path angle $\gamma = \theta - \alpha$, and heading rate $\dot{\psi} = (q \sin\phi + r \cos\phi)/\cos\theta$. Speed and glide path angle are inherently coupled for underwater gliders, just as they are for airplanes. For a *fixed* glide path angle, speed can be directly modulated by changing the net mass $\tilde{m}$. Changing $\tilde{m}$ requires pressure-volume work, however, which is relatively expensive, especially at depth. In practice, it is best to modulate $\tilde{m}$ as infrequently as possible. Here, we focus on controlling the glide path angle γ by varying the longitudinal moving mass position $r_{\rm px}$.

A sophisticated dynamic model presented in Section 2 has been used to design the feedback compensator. The model incorporates the buoyancy and moving mass actuator dynamics and servo-control laws. It is convenient to replace the velocity $\boldsymbol{v}$, as expressed in the body reference frame, with

speed, angle of attack, and sideslip angle (V, α, β). To do so, note that

$$\begin{aligned} \boldsymbol{v} &= e^{-\widehat{\boldsymbol{e}_2}\alpha} e^{\widehat{\boldsymbol{e}_3}\beta}(V\boldsymbol{e}_1) \\ \dot{\boldsymbol{v}} &= e^{-\widehat{\boldsymbol{e}_2}\alpha} e^{\widehat{\boldsymbol{e}_3}\beta} \begin{pmatrix} 1 & 0 & 0 \\ 0 & 0 & V \\ 0 & V\cos\beta & 0 \end{pmatrix} \begin{pmatrix} \dot{V} \\ \dot{\alpha} \\ \dot{\beta} \end{pmatrix}. \end{aligned}$$

The change of variables is well-defined for $\beta \in (-\frac{\pi}{2}, \frac{\pi}{2})$.

The equations of motion (7) can be written in the form

$$\mathbb{F}(\dot{\mathbb{X}}, \mathbb{X}, \mathbb{U}) = \mathbf{0}$$

where the system state and control vectors are

$$\mathbb{X} = \left[\phi, \theta, V, \alpha, \beta, p, q, r, r_{\mathrm{p_x}}, v_{\mathrm{p_x}}, r_{\mathrm{p_y}}, v_{\mathrm{p_y}}\right]^T \tag{11}$$

$$\mathbb{U} = \left[u_{\mathrm{p_x}}, u_{\mathrm{p_y}}, u_{\mathrm{b}}\right]^T. \tag{12}$$

Here, $v_{\mathrm{p_x}}$ and $v_{\mathrm{p_y}}$ represent the translational velocity of the moving masses relative to the inertial frame expressed in the body frame.

To design a servo-controller for the moving mass actuators and the variable ballast actuator, we linearize the dynamic equations about a wings-level equilibrium $(\mathbb{X}_0, \mathbb{U}_0)$ and compute the transfer function for each input-output channel of interest. Let U denote one of the available input signals $U \in \left\{u_{\mathrm{p_x}}, u_{\mathrm{p_y}}, u_{\mathrm{b}}\right\}$ and define a corresponding output $Y(\mathbb{X})$. With these definitions, we obtain the perturbation equations

$$\triangle\dot{\mathbb{X}} = \boldsymbol{A}\triangle\mathbb{X} + \boldsymbol{B}\triangle U \tag{13}$$

$$\triangle Y = \boldsymbol{C}\triangle\mathbb{X} \tag{14}$$

where

$$\begin{aligned} \boldsymbol{A} &= -\left[\left(\frac{\partial\mathbb{F}}{\partial\dot{\mathbb{X}}}\right)^{-1}\left(\frac{\partial\mathbb{F}}{\partial\mathbb{X}}\right)\right]_{\mathrm{eq}} \\ \boldsymbol{B} &= -\left[\left(\frac{\partial\mathbb{F}}{\partial\dot{\mathbb{X}}}\right)^{-1}\left(\frac{\partial\mathbb{F}}{\partial U}\right)\right]_{\mathrm{eq}} \\ \boldsymbol{C} &= \left[\frac{\partial Y}{\partial\mathbb{X}}\right]_{\mathrm{eq}} \end{aligned}$$

The matrix $\frac{\partial\mathbb{F}}{\partial\dot{\mathbb{X}}}$ is non-singular within the vehicle's normal performance envelope.

In designing moving mass servoactuator control laws, the objective is to choose an input $u_{\mathrm{p}} \in \{u_{\mathrm{p}_x}, u_{\mathrm{p}_y}\}$ such that the position of the moving mass $r_{\mathrm{p}} \in \{r_{\mathrm{p}_x}, r_{\mathrm{p}_y}\}$ asymptotically tracks a desired trajectory $r_{\mathrm{p_d}} \in \{r_{\mathrm{p}_{x_{\mathrm{d}}}}, r_{\mathrm{p}_{y_{\mathrm{d}}}}\}$. With $U = u_{\mathrm{p}}$ and $Y = r_{\mathrm{p}}$ in equations (13) and (14), the input U appears in the second derivative of the output Y. That is, the scalar $\boldsymbol{CB} = 0$ but $\boldsymbol{CAB}$ is nonzero. Let $e = r_{\mathrm{p_d}} - r_{\mathrm{p}}$ represent the error between the desired position of a moving mass and its current position and assume that $r_{\mathrm{p_d}}$ is twice differentiable. (The reference command can be filtered, if necessary, to ensure that it is suitably smooth.) In order to drive e to zero, one may choose

$$u_{\mathrm{p}} = \frac{1}{\mathbf{CAB}}(\ddot{r}_{\mathrm{p_d}} - \mathbf{CA}^2\triangle\mathbb{X} + [\omega_{\mathrm{n}}^2 \;\; 2\zeta\omega_{\mathrm{n}}]\mathbf{e})$$

where $\mathbf{e} = [e, \dot{e}]^T$ and where $\omega_{\rm n} \in \{\omega_{{\rm n}_x}, \omega_{{\rm n}_y}\}$ and $\zeta \in \{\zeta_x, \zeta_y\}$ are appropriately chosen control parameters.

To design a PID compensator to correct the feedforward commands, let $G(s)$ represent the transfer function for a particular control channel and let $G_{\rm c}(s)$ represent the PID controller:

$$G_c(s) = K_p(1 + \frac{1}{T_i s} + T_d s)$$

The proportional gain K_p, the integrator time T_i and the derivative time T_d are control parameters to be tuned by the control designer. In the time domain, the control signal is

$$r_{\rm p}^{\rm corr} = K_p e + K_i \int_{t_0}^{t} e(\tau) d\tau + K_d \dot{e}$$

where $K_i = K_p/T_i$ and $K_d = K_p T_d$. The error signal $e(t)$ measures the difference between the actual and commanded value of the output.

The approximate equilibrium value of $\tilde{r}_{\rm p_d} \in \{\tilde{r}_{{\rm p}_{x_{\rm d}}}, \tilde{r}_{{\rm p}_{y_{\rm d}}}\}$, as predicted by analytical solutions, is augmented with feedback compensation to compensate for approximation error:

$$r_{\rm p_d} \;=\; \tilde{r}_{\rm p_d} + r_{\rm p}^{\rm corr}.$$

To smooth the commanded parameter value so that the reference command to the internal servo-actuators is twice differentiable, we define a linear reference model:

$$F(s) : r_{\rm p_d} \to r_{\rm p_d}^{\rm comm} \qquad \text{where} \qquad F(s) = \frac{1}{(s/\omega_{\rm r})^2 + 2\zeta_{\rm r}(s/\omega_{\rm r}) + 1}$$

Equivalently, in time domain, define the following reference model dynamics for each servo-actuator:

$$\begin{aligned} \dot{\mathbf{z}} &= \begin{pmatrix} 0 & 1 \\ -\omega_{\rm r}^2 & -2\zeta_{\rm r}\omega_{\rm r} \end{pmatrix} \mathbf{z} + \begin{pmatrix} 0 \\ \omega_{\rm r}^2 \end{pmatrix} r_{\rm p_d} \\ r_{\rm p_d}^{\rm comm} &= \begin{pmatrix} 1 & 0 \end{pmatrix} \mathbf{z} \end{aligned}$$

where $r_{\rm p_d}(t) \in \{r_{{\rm p}_{x_{\rm d}}}(t), r_{{\rm p}_{y_{\rm d}}}(t)\}$ is the (possibly discontinuous) reference command to be filtered.

In physical implementations, the servo-actuation system is self-contained and there is no need to include it in the motion control system. Referring to the control system schematic in Figure 3, this reference command filter is internal to the system dynamics block appearing at the right. We include this element explicitly here in order to account for the full complexity of the multi-body mechanical system and to allow analysis of issues such as actuator magnitude and rate saturation. The natural frequency and damping ratio parameters in the reference model above may be chosen to accommodate actuator performance limitations through analysis and simulation.

For a *fixed* glide path angle, speed can be directly modulated by changing the net mass $\tilde{m}$. That is, given values θ_0 and γ_0, one may solve relation (9) for the corresponding values of $\tilde{m}_{\rm d}$. We design an input $u_{\rm b}$ such that the net mass $\tilde{m}$ asymptotically tracks a desired value $\tilde{m}_{\rm d}$. The simplest approach is to choose

$$u_{\rm b} = k_{\rm b} \left(\tilde{m}_{\rm d} - \tilde{m}\right)$$

where the constant $k_{\rm b}$ is chosen to accommodate the rate limit on $u_{\rm b}$.

6 Flight Path Control

We control the glide path angle γ by modulating the longitudinal moving mass position $r_{\mathrm{p_x}}$. Let $e_\gamma(t) = \gamma_\mathrm{d} - \gamma(t)$, where γ_d is the desired value of the glide path angle. The longitudinal moving mass reference signal is

$$r_{\mathrm{p_x}}^{\mathrm{corr}} = K_{p_\gamma} e_\gamma + K_{i_\gamma} \int_{t_0}^{t} e_\gamma(\tau) d\tau + K_{d_\gamma} \dot{e}_\gamma.$$

The first step is to tune the flight path controller for the linearized system dynamics. Having done so, the next step is to re-tune the controller as necessary for the nonlinear dynamics through simulation. Adding the result to the longitudinal moving mass position from the feedforward block gives the required position of the longitudinal moving mass to maintain a constant flight path angle:

$$r_{\mathrm{p_{x_d}}} \;=\; \tilde{r}_{\mathrm{p_{x_d}}} + r_{\mathrm{p_x}}^{\mathrm{corr}}$$

As explained in Section 3, we assume that the nominal gravitational moment is due entirely to $\mathbf{r}_{\mathrm{rb}}$ and that $\tilde{r}_{\mathrm{p_{x_d}}} = 0$. Hence, for $\gamma_\mathrm{d} = \gamma_0$, we have only the feedback term $r_{\mathrm{p_{x_d}}} = r_{\mathrm{p_x}}^{\mathrm{corr}}$.

The longitudinal moving mass actuator is subject to magnitude and rate limits due to the limited range of travel of the moving mass and the operational limits of the servomotor, respectively. To ensure a smooth reference trajectory, and to help accommodate the rate limit, one may filter the reference command as follows.

$$r_{\mathrm{p_{x_d}}}^{\mathrm{comm}} \;=\; \begin{pmatrix} 1 & 0 \end{pmatrix} \mathbf{z}_\mathrm{x} \;\text{ where }\; \dot{\mathbf{z}}_\mathrm{x} = \begin{pmatrix} 0 & 1 \\ -\omega_{\mathrm{r_x}}^2 & -2\zeta_{\mathrm{r_x}}\omega_{\mathrm{r_x}} \end{pmatrix} \mathbf{z}_\mathrm{x} + \begin{pmatrix} 0 \\ \omega_{\mathrm{r_x}}^2 \end{pmatrix} r_{\mathrm{p_{x_d}}}(t)$$

The input $u_{\mathrm{p_x}}$ guarantees that the position of the longitudinal moving mass $r_{\mathrm{p_x}}$ asymptotically tracks the (twice differentiable) trajectory $r_{\mathrm{p_{x_d}}}^{\mathrm{comm}}$ generated by filtering the (possibly discontinuous) desired value $r_{\mathrm{p_{x_d}}}$:

$$u_{\mathrm{p_x}} = \frac{(\ddot{r}_{\mathrm{p_{x_d}}}^{\mathrm{comm}} - \boldsymbol{C}_\mathrm{x}\boldsymbol{A}^2\boldsymbol{X} + [\omega_{\mathrm{n_x}}^2 \;\; 2\zeta_\mathrm{x}\omega_{\mathrm{n_x}}]\mathbf{e}_\mathrm{x})}{\boldsymbol{C}_\mathrm{x}\boldsymbol{A}\boldsymbol{B}_\mathrm{x}} \qquad \text{where} \qquad \boldsymbol{e}_\mathrm{x} = (e_\mathrm{x}, \dot{e}_\mathrm{x})^T \;\text{ and }\; e_\mathrm{x} = r_{\mathrm{p_{x_d}}}^{\mathrm{comm}} - r_{\mathrm{p_x}}$$

7 Turn Rate Control

The control channel from lateral mass position $r_{\mathrm{p_y}}^{\mathrm{corr}}$ to turn rate $\dot{\psi}$ is non-minimum phase, with a single zero in the right half plane. This non-minimum phase zero limits closed-loop bandwidth. In any case, closing the loop from turn rate to lateral mass location is effective, provided the performance limitations are respected in control parameter selection. Let $e_{\dot{\psi}}(t) = \dot{\psi}_\mathrm{d}(t) - \dot{\psi}(t)$, where $\dot{\psi}_\mathrm{d}(t)$ is the desired turn rate. The lateral moving mass control signal is

$$r_{\mathrm{p_y}}^{\mathrm{corr}} = K_{p_{\dot{\psi}}} e_{\dot{\psi}} + K_{i_{\dot{\psi}}} \int_{t_0}^{t} e_{\dot{\psi}}(\tau) d\tau + K_{d_{\dot{\psi}}} \dot{e}_{\dot{\psi}}.$$

The turn rate PID controller was first tuned for the linearized system dynamics, and then re-tuned for the nonlinear dynamics through simulation. Adding the result to the lateral moving

mass position from the feedforward block gives the required position of the lateral moving mass to maintain the desired turn rate.

$$r_{\mathrm{p_{y_d}}} \;=\; \tilde{r}_{\mathrm{p_{y_d}}} + r_{\mathrm{p_y}}^{\mathrm{corr}}$$

Again, the command is filtered to ensure a dynamically feasible reference:

$$r_{\mathrm{p_{y_d}}}^{\mathrm{comm}} \;=\; \begin{pmatrix} 1 & 0 \end{pmatrix} \mathbf{z}_{\mathrm{y}} \;\text{ where }\; \dot{\mathbf{z}}_{\mathrm{y}} = \begin{pmatrix} 0 & 1 \\ -\omega_{\mathrm{r_y}}^2 & -2\zeta_{\mathrm{r_y}}\omega_{\mathrm{r_y}} \end{pmatrix} \mathbf{z}_{\mathrm{y}} + \begin{pmatrix} 0 \\ \omega_{\mathrm{r_y}}^2 \end{pmatrix} r_{\mathrm{p_{y_d}}}(t)$$

The input $u_{\mathrm{p_y}}$ guarantees that the position of the lateral moving mass $r_{\mathrm{p_y}}$ asymptotically tracks the (twice differentiable) trajectory $r_{\mathrm{p_{y_d}}}^{\mathrm{comm}}$ generated by filtering (possibly discontinuous) desired value $r_{\mathrm{p_{y_d}}}$.

$$u_{\mathrm{p_y}} = \frac{(\ddot{r}_{\mathrm{p_{y_d}}}^{\mathrm{comm}} - \boldsymbol{C}_{\mathrm{y}}\boldsymbol{A}^2\boldsymbol{X} + [\omega_{\mathrm{n_y}}^2 \quad 2\zeta_{\mathrm{y}}\omega_{\mathrm{n_y}}]\mathbf{e}_{\mathrm{y}})}{\boldsymbol{C}_{\mathrm{y}}\boldsymbol{A}\boldsymbol{B}_{\mathrm{y}}} \qquad \text{where} \qquad \boldsymbol{e}_{\mathrm{y}} = (e_{\mathrm{y}}, \dot{e}_{\mathrm{y}})^T \;\text{ and }\; e_{\mathrm{y}} = r_{\mathrm{p_{y_d}}}^{\mathrm{comm}} - r_{\mathrm{p_y}}$$

8 Stability Analysis of Closed Loop System

To analyze this system, consider $\dot{\psi}_{\mathrm{d}}$ as a frozen parameter. For each fixed value the frozen system has an isolated equilibrium point. Consider the linearized equations about this equilibrium point:

$$\begin{aligned} \dot{\mathbb{X}} &= \boldsymbol{A}\mathbb{X} + \boldsymbol{B}_{\mathrm{y}} u_{\mathrm{p_y}} \\ r_{\mathrm{p_y}} &= \boldsymbol{C}_{\mathrm{y}}\mathbb{X} \end{aligned}$$

where $\mathbb{X}$ is the state vector given in (11). Defining the lateral mass error $e_{\mathrm{y}} = r_{\mathrm{p_{y_d}}}^{\mathrm{comm}} - r_{\mathrm{p_y}}$ and the heading rate error $e_{\dot{\psi}} = \dot{\psi}_{\mathrm{d}} - \dot{\psi}$, the input $u_{\mathrm{p_y}}$ is

$$u_{\mathrm{p_y}} = \frac{(\ddot{r}_{\mathrm{p_{y_d}}}^{\mathrm{comm}} - \boldsymbol{C}_{\mathrm{y}}\boldsymbol{A}^2\mathbb{X} + \begin{pmatrix} \omega_{\mathrm{n_y}}^2 & 2\zeta_{\mathrm{y}}\omega_{\mathrm{n_y}} \end{pmatrix} \mathbf{e}_{\mathrm{y}})}{\boldsymbol{C}_{\mathrm{y}}\boldsymbol{A}\boldsymbol{B}_{\mathrm{y}}} \qquad \text{where} \qquad \boldsymbol{e}_{\mathrm{y}} = (e_{\mathrm{y}}, \dot{e}_{\mathrm{y}})^T$$

$$r_{\mathrm{p_{y_d}}}^{\mathrm{comm}} \;=\; \begin{pmatrix} 1 & 0 \end{pmatrix} \mathbf{z}_{\mathrm{y}} \qquad \text{where} \qquad \dot{\mathbf{z}}_{\mathrm{y}} = \begin{pmatrix} 0 & 1 \\ -\omega_{\mathrm{r_y}}^2 & -2\zeta_{\mathrm{r_y}}\omega_{\mathrm{r_y}} \end{pmatrix} \mathbf{z}_{\mathrm{y}} + \begin{pmatrix} 0 \\ \omega_{\mathrm{r_y}}^2 \end{pmatrix} r_{\mathrm{p_{y_d}}}$$

$$r_{\mathrm{p_{y_d}}} \;=\; \tilde{r}_{\mathrm{p_{y_d}}} + r_{\mathrm{p_y}}^{\mathrm{corr}} \qquad \text{with} \qquad r_{\mathrm{p_y}}^{\mathrm{corr}} = K_{p_{\dot{\psi}}} e_{\dot{\psi}} + K_{i_{\dot{\psi}}} z_{\dot{\psi}} + K_{d_{\dot{\psi}}} \dot{e}_{\dot{\psi}} \qquad \text{where} \qquad \dot{z}_{\dot{\psi}} = e_{\dot{\psi}}$$

Putting all the parts together, we have

$$\begin{aligned} \dot{\mathbb{X}} &= \boldsymbol{A}\mathbb{X} + \boldsymbol{B}_{\mathrm{y}} u_{\mathrm{p_y}} \\ \dot{\mathbf{z}}_{\mathrm{y}} &= \begin{pmatrix} 0 & 1 \\ -\omega_{\mathrm{r_y}}^2 & -2\zeta_{\mathrm{r_y}}\omega_{\mathrm{r_y}} \end{pmatrix} \mathbf{z}_{\mathrm{y}} + \begin{pmatrix} 0 \\ \omega_{\mathrm{r_y}}^2 \end{pmatrix} (\tilde{r}_{\mathrm{p_{y_d}}} + K_{p_{\dot{\psi}}} e_{\dot{\psi}} + K_{i_{\dot{\psi}}} z_{\dot{\psi}} + K_{d_{\dot{\psi}}} \dot{e}_{\dot{\psi}}) \\ \dot{z}_{\dot{\psi}} &= \dot{\psi}_d - \dot{\psi} \end{aligned}$$

where

$$
\begin{aligned}
u_{\mathrm{p_y}} &= \frac{1}{\boldsymbol{C}_{\mathrm{y}}\boldsymbol{A}\boldsymbol{B}_{\mathrm{y}}}\left[\begin{pmatrix} 0 & 1 \end{pmatrix}\dot{\mathbf{z}}_{\mathrm{y}} - \boldsymbol{C}_{\mathrm{y}}\boldsymbol{A}^2\mathbb{X} + \begin{pmatrix} \omega_{\mathrm{n_y}}^2 & 2\zeta_{\mathrm{y}}\omega_{\mathrm{n_y}} \end{pmatrix}\begin{pmatrix} \begin{pmatrix} 1 & 0 \end{pmatrix}\mathbf{z}_{\mathrm{y}} - r_{\mathrm{p_y}} \\ \begin{pmatrix} 1 & 0 \end{pmatrix}\dot{\mathbf{z}}_{\mathrm{y}} - v_{\mathrm{p_y}} \end{pmatrix}\right] \\
&= \frac{1}{\boldsymbol{C}_{\mathrm{y}}\boldsymbol{A}\boldsymbol{B}_{\mathrm{y}}}\left[-\begin{pmatrix} \omega_{\mathrm{r_y}}^2 & 2\zeta_{\mathrm{r_y}}\omega_{\mathrm{r_y}} \end{pmatrix}\mathbf{z}_{\mathrm{y}} + \omega_{\mathrm{r_y}}^2[\tilde{r}_{\mathrm{p_{y_d}}} + \begin{pmatrix} K_{p_{\dot\psi}} & K_{d_{\dot\psi}} \end{pmatrix}\begin{pmatrix} e_{\dot\psi} \\ \dot{e}_{\dot\psi} \end{pmatrix} + K_{i_{\dot\psi}}z_{\dot\psi}]\right] \\
&\quad + \frac{1}{\boldsymbol{C}_{\mathrm{y}}\boldsymbol{A}\boldsymbol{B}_{\mathrm{y}}}\left[\begin{pmatrix} \omega_{\mathrm{n_y}}^2 & 2\zeta_{\mathrm{y}}\omega_{\mathrm{n_y}} \end{pmatrix}\mathbf{z}_{\mathrm{y}} - \begin{pmatrix} \omega_{\mathrm{n_y}}^2 & 2\zeta_{\mathrm{y}}\omega_{\mathrm{n_y}} \end{pmatrix}\begin{pmatrix} r_{\mathrm{p_y}} \\ v_{\mathrm{p_y}} \end{pmatrix} - \boldsymbol{C}_{\mathrm{y}}\boldsymbol{A}^2\mathbb{X}\right] \\
&= \frac{1}{\boldsymbol{C}_{\mathrm{y}}\boldsymbol{A}\boldsymbol{B}_{\mathrm{y}}}\left[\omega_{\mathrm{r_y}}^2\tilde{r}_{\mathrm{p_{y_d}}} + \omega_{\mathrm{r_y}}^2\begin{pmatrix} K_{p_{\dot\psi}} & K_{d_{\dot\psi}} \end{pmatrix}\begin{pmatrix} e_{\dot\psi} \\ \dot{e}_{\dot\psi} \end{pmatrix} - \begin{pmatrix} \omega_{\mathrm{n_y}}^2 & 2\zeta_{\mathrm{y}}\omega_{\mathrm{n_y}} \end{pmatrix}\begin{pmatrix} r_{\mathrm{p_y}} \\ v_{\mathrm{p_y}} \end{pmatrix}\right] \\
&\quad + \frac{1}{\boldsymbol{C}_{\mathrm{y}}\boldsymbol{A}\boldsymbol{B}_{\mathrm{y}}}\left[\begin{pmatrix} -1 & 1 \end{pmatrix}\begin{pmatrix} \omega_{\mathrm{r_y}}^2 & 2\zeta_{\mathrm{r_y}}\omega_{\mathrm{r_y}} \\ \omega_{\mathrm{n_y}}^2 & 2\zeta_{\mathrm{y}}\omega_{\mathrm{n_y}} \end{pmatrix}\mathbf{z}_{\mathrm{y}} + \omega_{\mathrm{r_y}}^2 K_{i_{\dot\psi}}z_{\dot\psi} - \boldsymbol{C}_{\mathrm{y}}\boldsymbol{A}^2\mathbb{X}\right]
\end{aligned}
$$

Define $\boldsymbol{C}_{\dot\psi}$ so that $\boldsymbol{C}_{\dot\psi}\mathbb{X} = \begin{pmatrix} e_{\dot\psi} & \dot{e}_{\dot\psi} \end{pmatrix}^T$ and $\boldsymbol{C}_{\mathrm{p_y}}$ so that $\boldsymbol{C}_{\mathrm{p_y}}\mathbb{X} = \begin{pmatrix} r_{\mathrm{p_y}} & v_{\mathrm{p_y}} \end{pmatrix}^T$.

For a given "frozen" value of the commanded turn rate $\dot\psi_{\mathrm{d}}$, we denote the equilibrium point for the complete system $\mathbf{h}(\dot\psi_{\mathrm{d}}) = (\mathbb{X}_{\mathrm{eq}}^T, \mathbf{z}_{\mathrm{y_{eq}}}^T, z_{\dot\psi_{\mathrm{eq}}})^T$. One may verify that

$$
\|\frac{\partial \mathbf{h}}{\partial \dot\psi_{\mathrm{d}}}\| \leq L \tag{15}
$$

for some positive constant $L > 0$. This important condition guarantees that the equilibrium state "varies nicely" with the slowly varying turn rate command $\dot\psi_{\mathrm{d}}$. To analyze stability, we change variables so that the equilibrium is at the origin in the new variables:

$$
\acute{\boldsymbol{x}} = (\acute{\mathbb{X}}^T, \acute{\mathbf{z}}_{\mathrm{y}}^T, \acute{z}_{\dot\psi})^T = (\mathbb{X}^T, \mathbf{z}_{\mathrm{y}}^T, z_{\dot\psi})^T - \mathbf{h}(\dot\psi_{\mathrm{d}})
$$

The complete linearized equations are

$$
\begin{aligned}
\dot{\acute{\mathbb{X}}} &= \left[\boldsymbol{A} + \boldsymbol{B}_{\mathrm{y}}\frac{1}{\boldsymbol{C}_{\mathrm{y}}\boldsymbol{A}\boldsymbol{B}_{\mathrm{y}}}\left[\omega_{\mathrm{r_y}}^2\begin{pmatrix} K_{p_{\dot\psi}} & K_{d_{\dot\psi}} \end{pmatrix}\boldsymbol{C}_{\dot\psi} - \begin{pmatrix} \omega_{\mathrm{n_y}}^2 & 2\zeta_{\mathrm{y}}\omega_{\mathrm{n_y}} \end{pmatrix}\boldsymbol{C}_{\mathrm{p_y}} - \boldsymbol{C}_{\mathrm{y}}\boldsymbol{A}^2\right]\right]\acute{\mathbb{X}} \\
&\quad + \boldsymbol{B}_{\mathrm{y}}\frac{1}{\boldsymbol{C}_{\mathrm{y}}\boldsymbol{A}\boldsymbol{B}_{\mathrm{y}}}\left[\begin{pmatrix} -1 & 1 \end{pmatrix}\begin{pmatrix} \omega_{\mathrm{r_y}}^2 & 2\zeta_{\mathrm{r_y}}\omega_{\mathrm{r_y}} \\ \omega_{\mathrm{n_y}}^2 & 2\zeta_{\mathrm{y}}\omega_{\mathrm{n_y}} \end{pmatrix}\right]\acute{\mathbf{z}}_{\mathrm{y}} + \boldsymbol{B}_{\mathrm{y}}\frac{1}{\boldsymbol{C}_{\mathrm{y}}\boldsymbol{A}\boldsymbol{B}_{\mathrm{y}}}\omega_{\mathrm{r_y}}^2 K_{i_{\dot\psi}}\acute{z}_{\dot\psi} \\
\dot{\acute{\mathbf{z}}}_{\mathrm{y}} &= \begin{pmatrix} 0 \\ \omega_{\mathrm{r_y}}^2 \end{pmatrix}\begin{pmatrix} K_{p_{\dot\psi}} & K_{d_{\dot\psi}} \end{pmatrix}\boldsymbol{C}_{\dot\psi}\acute{\mathbb{X}} + \begin{pmatrix} 0 & 1 \\ -\omega_{\mathrm{r_y}}^2 & -2\zeta_{\mathrm{r_y}}\omega_{\mathrm{r_y}} \end{pmatrix}\acute{\mathbf{z}}_{\mathrm{y}} + \begin{pmatrix} 0 \\ \omega_{\mathrm{r_y}}^2 \end{pmatrix}K_{i_{\dot\psi}}\acute{z}_{\dot\psi} \\
\dot{\acute{z}}_{\dot\psi} &= \begin{pmatrix} -1 & 0 \end{pmatrix}\boldsymbol{C}_{\dot\psi}\acute{\mathbb{X}}
\end{aligned} \tag{16}
$$

More compactly, we write

$$
\dot{\acute{\boldsymbol{x}}} = \acute{\boldsymbol{A}}\acute{\boldsymbol{x}}
$$

where the elements of $\acute{\boldsymbol{A}}$ are continuously differentiable functions of $\dot\psi_{\mathrm{d}} \in \Gamma = [0, a)$, where a is the maximum turn rate for the underwater glider. Suppose that $\acute{\boldsymbol{A}}$ is Hurwitz uniformly in $\dot\psi_{\mathrm{d}}$. That is, suppose the controller has been designed such that every eigenvalue λ in the spectrum of $\acute{\boldsymbol{A}}$ satisfies

$$
\mathrm{Re}(\lambda) \leq -\sigma < 0 \qquad \forall\, \dot\psi_{\mathrm{d}} \in \Gamma
$$

for some positive constant σ. Then, from Lemma 9.9 in [15] the Lyapunov equation

$$\mathbf{P}\acute{\boldsymbol{A}} + \acute{\boldsymbol{A}}^T\mathbf{P} = -\mathbb{I}.$$

has a unique positive definite solution $\mathbf{P}$ for every $\dot{\psi}_\mathrm{d} \in \Gamma$. $\mathbf{P}(\dot{\psi}_\mathrm{d})$ is continuously differentiable and satisfies

$$\begin{aligned} c_1\acute{\boldsymbol{x}}^T\acute{\boldsymbol{x}} \;\leq\; \acute{\boldsymbol{x}}^T\,\mathbf{P}(\dot{\psi}_\mathrm{d})\,\acute{\boldsymbol{x}} \;\leq\; c_2\acute{\boldsymbol{x}}^T\acute{\boldsymbol{x}} \\ \|\frac{\partial}{\partial\dot{\psi}_\mathrm{d}}\mathbf{P}(\dot{\psi}_\mathrm{d})\| \;\leq\; \vartheta \end{aligned}$$

for all $(\acute{\boldsymbol{x}}, \dot{\psi}_\mathrm{d}) \in \mathbb{R}^n \times \Gamma$, where c_1, c_2, and ϑ are positive constants independent of $\dot{\psi}_\mathrm{d}$. Consequently, there exists some $r > 0$ such that the Lyapunov function $V(\acute{\boldsymbol{x}}, \dot{\psi}_\mathrm{d}) = \acute{\boldsymbol{x}}^T\,\mathbf{P}\,\acute{\boldsymbol{x}}$ satisfies the following inequalities

$$\begin{aligned} c_1\|\acute{\boldsymbol{x}}\|^2 \;\leq\; V(\acute{\boldsymbol{x}}, \dot{\psi}_\mathrm{d}) \;\leq\; c_2\|\acute{\boldsymbol{x}}\|^2 \\ \|\frac{\partial V}{\partial\acute{\boldsymbol{x}}}\|g(\acute{\boldsymbol{x}}, \dot{\psi}_\mathrm{d}) \;\leq\; -c_3\|\acute{\boldsymbol{x}}\|^2 \\ \|\frac{\partial V}{\partial\acute{\boldsymbol{x}}}\| \;\leq\; c_4\|\acute{\boldsymbol{x}}\| \\ \|\frac{\partial V}{\partial\dot{\psi}_\mathrm{d}}\| \;\leq\; c_5\|\acute{\boldsymbol{x}}\|^2 \end{aligned}$$

for all $\acute{\boldsymbol{x}} \in D = \{\acute{\boldsymbol{x}} \in \mathbb{R}^n | \|\acute{\boldsymbol{x}}\| < r\}$ and $\dot{\psi}_\mathrm{d} \in \Gamma$. We may choose the positive constants $c_1 = \lambda_{\min}(\mathbf{P})$, $c_2 = \lambda_{\max}(\mathbf{P})$, $c_3 = 1$, $c_4 = 2\lambda_{\max}(\mathbf{P})$, and $c_5 = 0$ (Lemma 9.9 in [15]). Trajectories $\acute{\boldsymbol{x}}(t)$ are uniformly ultimately bounded with an ultimate bound proportional to ε, the bound on the turn acceleration. An upper bound on the value of ε can be computed from the following requirement:

$$\| \ddot{\psi}_\mathrm{d}(t) \| \leq \varepsilon < \frac{c_1c_3}{c_2} \times \frac{r}{rc_5 + c_4L} \tag{17}$$

By Theorem 9.3 in [15], the norm of the tracking error remains smaller than $k\varepsilon$ for some finite $k > 0$. Moreover, if $\ddot{\psi}_\mathrm{d}(t) \to 0$ as $t \to \infty$, the tracking error tends to zero.

Solving the Lyapunov equation and calculating the eigenvalues of $\mathbf{P}$ one obtains the c_i, $i = 1, 2, \ldots, 5$ and an upper bound for ε, the limit for commanded turn accelerations. Applying the proposed motion control system to the *Slocum* model given in [2], and performing the analysis outlined above, one obtains the constants:

$$c_1 = \lambda_{\min}(\mathbf{P}) = -378.75, \quad c_2 = \lambda_{\max}(\mathbf{P}) = 979.82, \quad c_3 = 1, \quad c_4 = 2\lambda_{\max}(\mathbf{P}), \quad \text{and} \quad c_5 = 0.$$

which gives

$$|\ddot{\psi}_\mathrm{d}(t)| \leq \varepsilon < 2 \times 10^{-4}\frac{r}{L}$$

This is a conservative upper bound for acceleration in turn rate reference commands. A relaxed bound could be obtained by applying similar analysis in the time varying setting. (See Theorems 7.4 and 7.8 in [23], for example.)

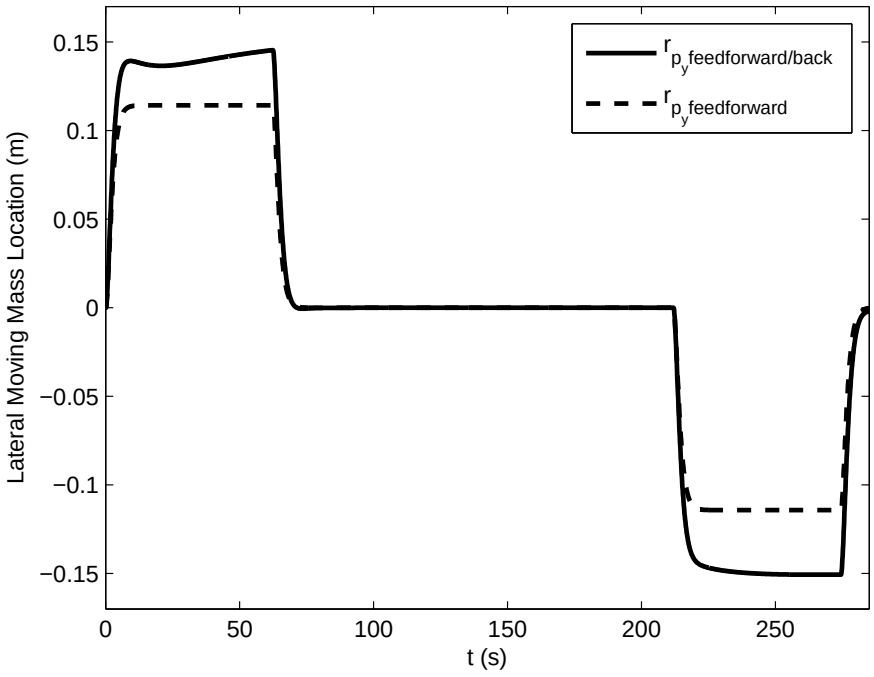

Figure 4: Lateral moving mass location (open- and closed-loop).

9 Simulation Results

A sophisticated glider model based on the *Slocum* model given in [2] was linearized about the following equilibrium flight condition, which corresponds to wings-level, descending flight:

$$V_0 = 0.77 \text{ m/s}, \quad \alpha_0 = 4.3^\circ, \quad \theta_0 = -8.4^\circ, \quad \gamma_0 = -12.7^\circ, \quad \text{and} \quad \tilde{m}_0 = 0.63 \text{ kg}.$$

The moving mass values are $m_{\mathrm{p_x}} = m_{\mathrm{p_y}} = 9$ kg. The servo-actuator parameter values are

$$\begin{aligned} \omega_{\mathrm{n_x}} &= 20 \text{ rad/s}, \quad \zeta_{\mathrm{x}} = 0.001, \quad \omega_{\mathrm{r_x}} = 0.8 \text{ rad/s}, \quad \text{and} \quad \zeta_{\mathrm{r_x}} = 1 \\ \omega_{\mathrm{n_y}} &= 20 \text{ rad/s}, \quad \zeta_{\mathrm{y}} = 0.01, \quad \omega_{\mathrm{r_y}} = 0.8 \text{ rad/s}, \quad \text{and} \quad \zeta_{\mathrm{r_y}} = 1 \end{aligned}$$

The PID control parameter values are

$$\begin{aligned} K_{p_\gamma} &= -0.2 \text{ m}, \quad T_{i_\gamma} = 2.3 \text{ s}, \quad \text{and} \quad T_{d_\gamma} = 2 \text{ s} \\ K_{p_{\dot\psi}} &= 0.2 \text{ m/(rad/s)}, \quad T_{i_{\dot\psi}} = 0.65 \text{ s}, \quad \text{and} \quad T_{d_{\dot\psi}} = 0.39 \text{ s} \end{aligned}$$

Figures 4 through 8 compare the results of simulations using feedforward and feedforward/feedback control. Figure 4 shows the lateral mass location in response to a command sequence that is intended to effect a right turn, a straight segment, and a left turn (viewed from above) from an initial point to a desired final point. In the open-loop case (feedforward only), the moving mass is simply commanded to move to the (approximate) equilibrium value corresponding to a desired heading rate $\dot{\psi}_{\mathrm{d}}$. In the closed-loop case (feedforward/feedback), however, the heading rate is directly commanded, with the lateral moving mass actuator responding as necessary. The resulting path is depicted in Figure 5.

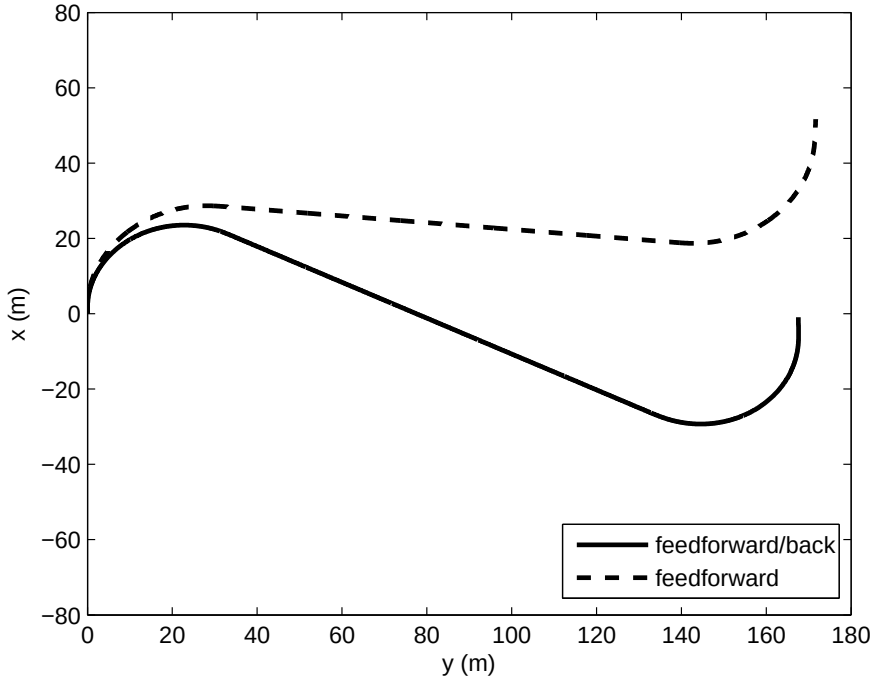

Figure 5: *Slocum* path in response to command sequence.

Figures 6 and 7 show desired, open-loop, and closed-loop value of the vehicle's glide path angle and turn rate. As expected, the deviation between the open-loop values and the desired values is significant. In Figure 7, the small spikes at the end of each segment correspond to reaction forces due to the movement of the lateral mass within the vehicle. We note that the turn rate magnitudes are of the same order as turn rates seen in glider operations. The *Slocum* glider, for example, can achieve a 20-30 m turn radius at speeds on the order of 0.5 m/s. A shallow-water variant of *Slocum*, which includes a movable rudder, can perform turns with a 7 m radius [3]. Figure 8 shows the location of the longitudinal moving mass, which regulates the glide path angle.

Remark 9.1 *The path in Figure 5 is reminiscent of a Dubins path, although the vehicle and actuator dynamics are included here. Time-optimal paths for a Dubins car with acceleration limits are discussed in [16] and [24], where it is recognized that extremal paths comprise sequences of straight, clothoidal, and circular segments.*

It must be stressed that the final guidance loop has not been closed, at this point. That is, we have not presented a control law to make the vehicle track a commanded *path*, such as a suboptimal Dubins path. Rather, we have presented the underlying motion control system over which a guidance loop might be imposed.

Figures 9 through 11 compare results of the simulation for the common feedback motion control system and the feedforward/feedback motion control system presented in this work. Figure 9 shows that the steady-motion based feedforward/feedback system reaches the desired turn rate much faster. Hence, the vehicle reaches the desired final point in shorter time (Figure 11). Figure 10 illustrates the effectiveness of both control loops in maintaining a constant flight path angle.

Comparing results of the simulations, for the three cases of feedforward, feedback, and feedfor-

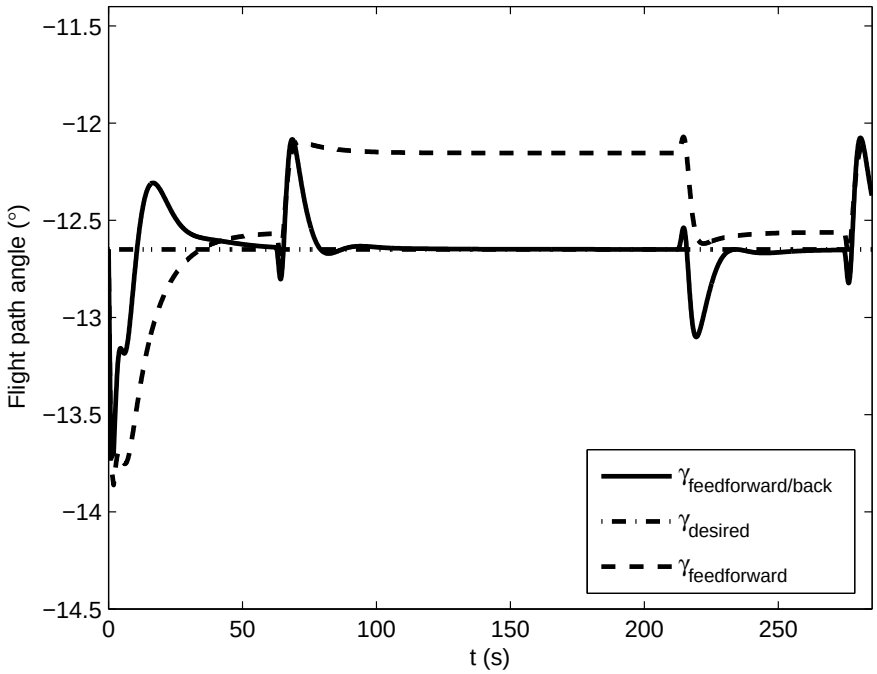

Figure 6: Glide path angle response to command sequence.

ward/feedback controller, shows that there is large error in turn rate when using just feedforward controller (Figure 7) which corresponds to large error in the resultant path (Figure 5). Figure 11 shows that the feedback controller is slow but precise; it takes longer time and larger distance to achieve desired turn rate (Figure 11). The combination, the proposed feedforward/feedback controller, illustrates fast, precise tracking of the commanded turn rate. Since the control system relies largely on steady motions, it is intrinsically efficient.

10 Conclusions

Building on prior results in glider steady motion analysis, a feedforward/feedback motion control system was presented to control speed, glide path angle, and turn rate. The control system uses feedforward commands obtained from an approximate solution for steady turning motion and includes feedback to compensate for approximation error and other uncertainties. The control system design includes model reference controllers for the servo-actuators, to allow actuator rate and magnitude saturation effects to be more easily analyzed and accommodated. Stability of the closed-loop system was analyzed using slowly varying systems theory in which the turn rate command was treated as a slowly varying parameter. A bound on turn acceleration was obtained as a product of the analysis. The controller's effectiveness was demonstrated in a simulation of a multi-body model of the underwater glider *Slocum*.

The proposed control system provides a mechanism for path following. The next step is to implement a guidance strategy, together with a path planning strategy, and one which continues to exploit the natural efficiency of this class of vehicle. The structure of the approximate solution for steady turning motion is such that, to first order in turn rate, the glider's horizontal component of motion

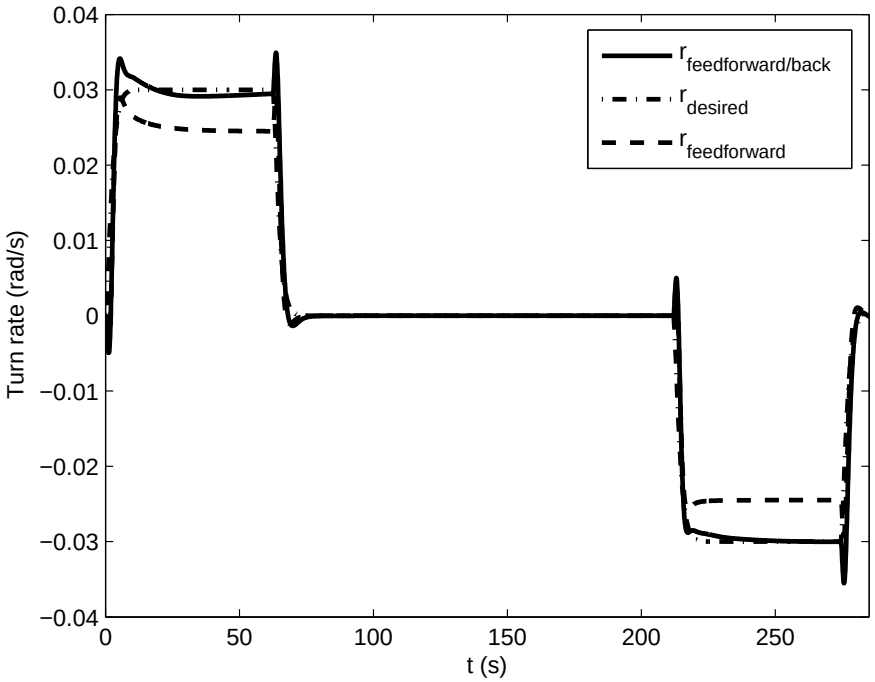

Figure 7: Turn rate response to command sequence.

matches that of the "Dubins car," a kinematic car with bounded turn rates. The Dubins car is a classic example in the study of time-optimal control for mobile robots. For an underwater glider, one can relate time optimality to energy optimality. Specifically, for an underwater glider travelling at a constant speed and maximum flight efficiency (i.e., maximum lift-to-drag ratio), minimum time paths are minimum energy paths. Hence, energy-efficient paths can be obtained by generating sequences of steady wings-level and turning motions. These efficient paths can, in turn, be followed using the motion control system described here.

In closing, we note that the feedforward component of the proposed control system, as presented, relies on the analytical solution for the steady turning motions of an underwater glider. This analysis is based on a sophisticated model of the underwater glider dynamics. In the absence of such a model, and the corresponding solution for steady motions, one may instead use a look-up table which maps vehicle configurations to stable, steady motions. Although such a table would have to be developed through an exhaustive series of experimental sea trials, the approach may, in some cases, be more expedient than developing a complete dynamic model.

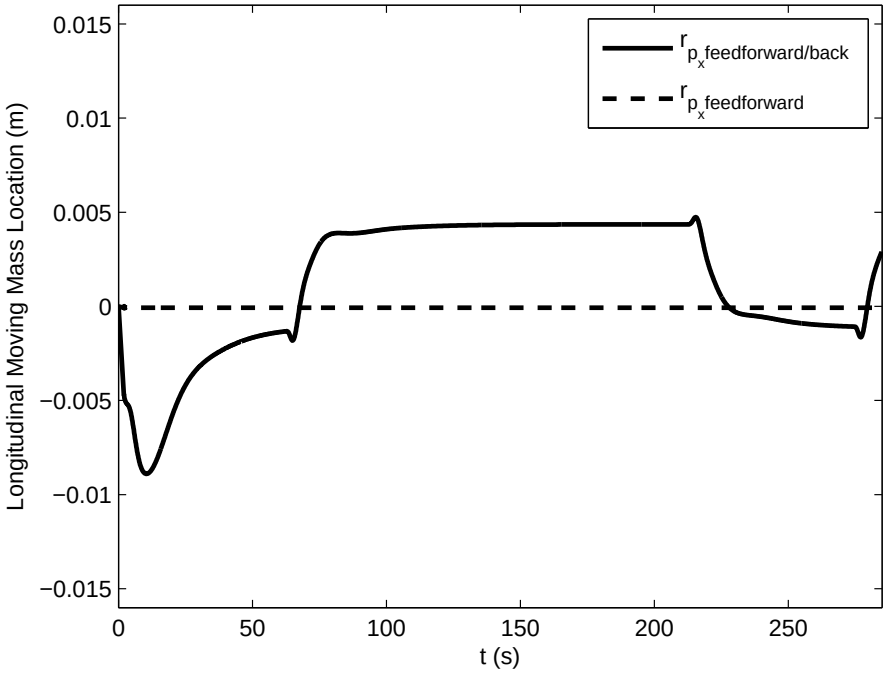

Figure 8: Variation in longitudinal moving mass position from nominal.

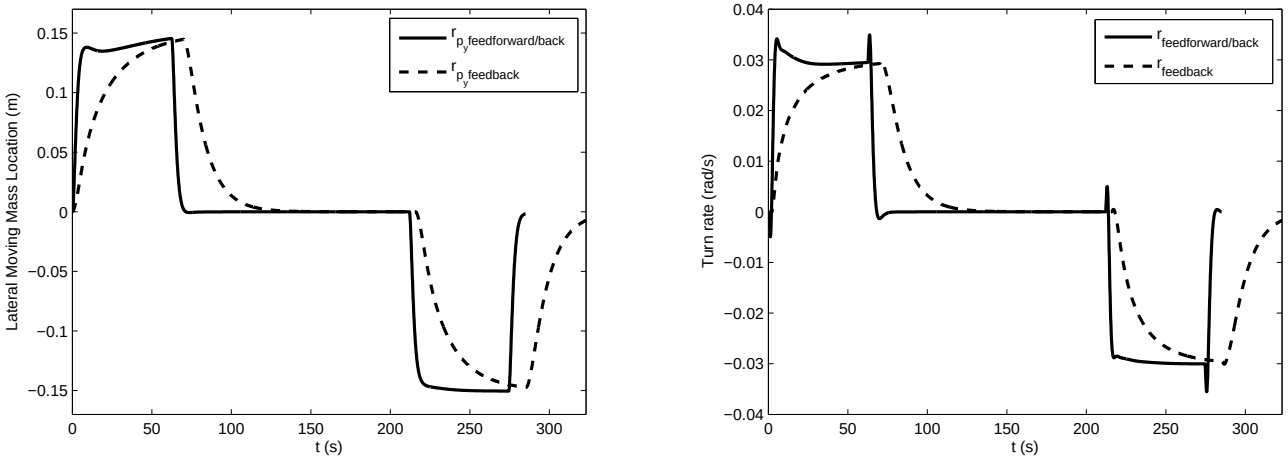

Figure 9: Lateral moving mass position and turn rate.

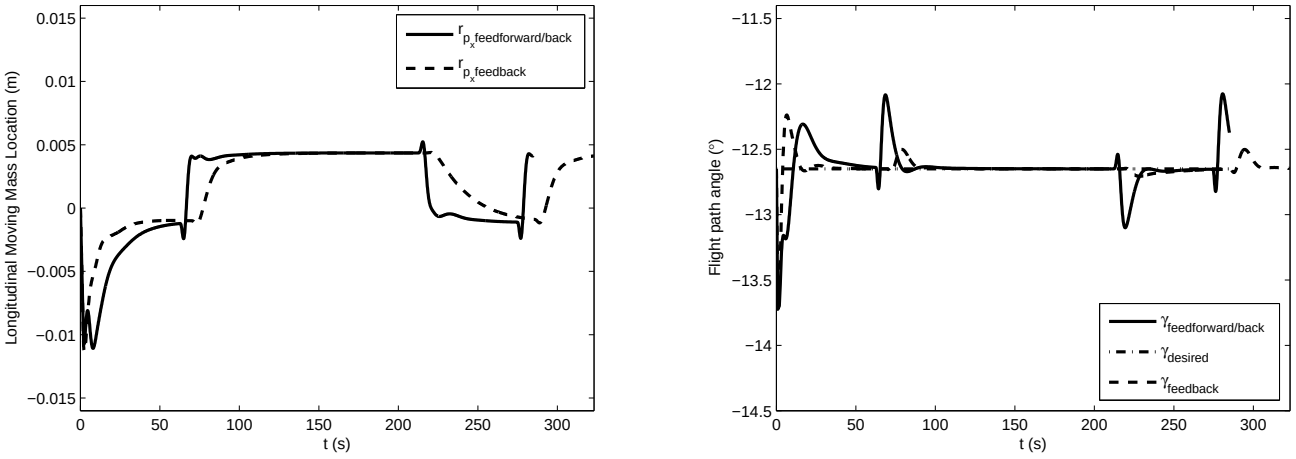

Figure 10: Longitudinal moving mass position and flight path angle.

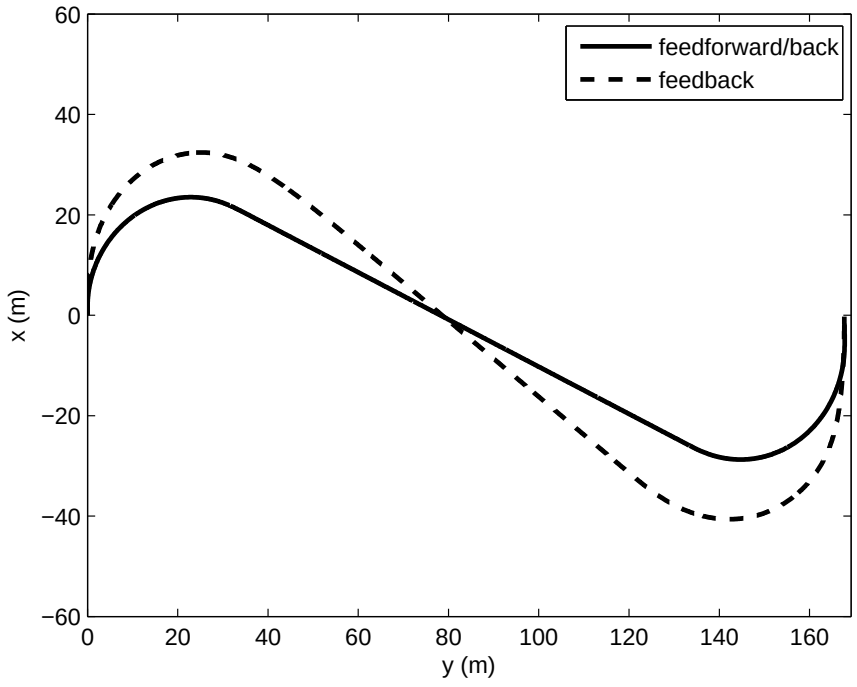

Figure 11: *Slocum* path in response to feedback and feedforward/feedback compensator.

References

[1] R. Bachmayer, J.G. Graver, and N. E. Leonard. Glider control: A close look into the current glider controller structure and future developments. In *IEEE Oceans 2003*, volume 2, pages 951–954, 2003.

[2] P. Bhatta. *Nonlinear Stability and Control of Gliding Vehicles*. PhD thesis, Princeton University, 2006.

[3] R. E. Davis, C. C. Eriksen, and C. P. Jones. Autonomous buoyancy-driven underwater gliders. In G. Griffiths, editor, *Technology and Applications of Autonomous Underwater Vehicles*, volume 2, chapter 3. Taylor and Francis, 2002.

[4] C. C. Eriksen, T. J. Osse, R. D. Light, T. Wen, T. W. Lehman, P. L. Sabin, J. W. Ballard, and A. M. Chiodi. Seaglider: A long-range autonomous underwater vehicle for oceanographic research. *Journal of Oceanic Engineering*, 26(4):424–436, 2001. Special Issue on Autonomous Ocean-Sampling Networks.

[5] T. I. Fossen. *Guidance and Control of Ocean Vehicles*. John Wiley and Sons, 1995.

[6] A. M. Galea. Optimal path planning and high level control of an autonomous gliding underwater vehicle. Master's thesis, Massachusetts Institute of Technology, 1999.

[7] J. S. Geisbert. Hydrodynamic modeling for autonomous underwater vehicles using computational and semi-empirical methods. Master's thesis, Virginia Polytechnic Institute & State University, Blacksburg, VA, June 2007.

[8] J. G. Graver. *Underwater Gliders: Dynamics, Control, and Design*. PhD thesis, Princeton University, 2005.

[9] J. G. Graver, J. Liu, C. A. Woolsey, and N. E. Leonard. Design and analysis of an underwater glider for controlled gliding. In *Conference on Information Sciences and Systems*, pages 801–806, 1998.

[10] J. Guckenheimer and P. Holmes. *Nonlinear Oscillations, Dynamical Systems, and Bifurcations of Vector Fields*. Springer-Verlag, New York, NY, 1983.

[11] P. Hartman. *Ordinary Differential Equations*. John Wiley and Sons, Inc., New York, NY, 1964.

[12] Sandra Hines. Seaglider monitors waters from arctic during record-breaking journey under ice. *EurekAlert*, April 28 2009. Available at `http://www.eurekalert.org/pub-releases/2009-04/uow-smw042809.php`.

[13] S. A. Jenkins, D. E. Humphreys, J. Sherman, J. Osse, C. Jones, N. Leonard, J. Graver, R. Bachmayer, T. Clem, P. Carroll, P. Davis, J. Berry, P. Worley, and J. Wasyl. Underwater glider system study. Technical Report 53, Scripps Institution of Oceanography, May 2003.

[14] C. Jones, D. Webb, S. Glenn, O. Schofield, J. Kerfoot, J. Kohut, H. Roarty, D. Aragon, C. Haldeman, T. Haskin, and A. Kahl. Slocum glider extending the endurance. Durham, NH, August 23-26 2009. The 16th International Symposium on Unmanned Untethered Submersible Technology (UUST09).

[15] H. K. Khalil. *Nonlinear Systems*. Prentice Hall, Upper Saddle River, NJ, third edition, 2002.

[16] V. Kostov and E. Degtiariova-Kostova. Suboptimal paths in the problem of a planar motion with bounded derivative of the curvature. Technical Report 2051, Institut National de Recherche en Informatique et en Automatique (INRIA), July 1993.

[17] N. E. Leonard and J. G. Graver. Model-based feedback control of autonomous underwater gliders. *Journal of Oceanic Engineering*, 26(4):633–645, 2001. Special Issue on Autonomous Ocean-Sampling Networks.

[18] N. Mahmoudian and C. Woolsey. Analysis of feedforward/feedback control design for underwater gliders based on slowly varying systems theory. Chicago, IL, Aug 20-23 2009. AIAA Guidance, Navigation and Control Conference and Exhibit.

[19] N. Mahmoudian, C. Woolsey, and J. Geisbert. Steady turns and optimal path for underwater gliders. Hilton Head, SC, Aug 20-23 2007. AIAA Guidance, Navigation and Control Conference and Exhibit.

[20] N. Mahmoudian and C. A. Woolsey. Underwater glider motion control. In *IEEE Conference on Decision and Control*, pages 552 – 557, Cancun, Mexico, December 2008.

[21] Nina Mahmoudian. *Efficient Motion Planning and Control for Underwater Gliders*. PhD thesis, Virginia Tech, 2009.

[22] Matt Mientka. Gliders flying onto the world's scientific stage more improvements planned. *Unmanned Systems*, 27(1):22 – 23, January 2009.

[23] W. J. Rugh. *Linear System Theory*. Prentice Hall, Upper Saddle River, NJ, second edition, 1996.

[24] A. Scheuer and Ch. Laugier. Planning sub-optimal and continuous-curvature paths for car-like robots. In *IEEE/RSJ International Conference on Intelligent Robots and Systems*, pages 25–31, Victoria, B.C., Canada, October 1998.

[25] J. Sherman, R. E. Davis, W. B. Owens, and J. Valdes. The autonomous underwater glider "Spray". *Journal of Oceanic Engineering*, 26(4):437–446, 2001. Special Issue on Autonomous Ocean-Sampling Networks.

[26] D. C. Webb, P. J. Simonetti, and C. P. Jones. SLOCUM: An underwater glider propelled by environmental energy. *Journal of Oceanic Engineering*, 26(4):447–452, 2001. Special Issue on Autonomous Ocean-Sampling Networks.

[27] C. A. Woolsey. Reduced Hamiltonian dynamics for a rigid body/mass particle system. *Journal of Guidance, Control, and Dynamics*, 28(1):131–138, January-February 2005.